Targeted delivery of niclosamide to FRβ-expressing macrophages with engineered 2-deoxy glucose dendrimer alleviates endometriosis progression and associated hyperalgesia.

Anubhav Dhull[1#], Mingxin Shi[2#], Madeleine E. Harvey[2#], Taylor M. Page[2], Rishi Sharma[1], Kenneth John Goody[1], Aqib Iqbal Dar[1], Nash S. Moawad[3], Vijay Kumar Sirohi[4], Paul S. Cooke[4], Kanako Hayashi[2]*, Anjali Sharma[1]*

[1]*Department of Chemistry, College of Arts and Sciences, Washington State University, 1470 NE College Ave, Pullman, WA 99164, USA.*

[2]*School of Molecular Biosciences, Center for Reproductive Biology, Washington State University, 1770 NE Stadium Way, Pullman, WA 99164, USA.*

[3]*Department of Obstetrics & Gynecology, University of Florida College of Medicine, P.O. Box 100294, Gainesville, FL 32610, USA.*

[4]*Department of Physiological Sciences, University of Florida, P.O. Box 100144, Gainesville, FL 32611, USA.*

[#]*These authors contributed equally to this work*

*Correspondence:

Anjali Sharma, Department of Chemistry, Washington State University, Troy Hall, Rm 222, 1470 E. College Avenue, Pullman, WA 99164, USA.

Hayashi Kanako, School of Molecular Biosciences, Washington State University, Biotechnology-Life Sciences, Rm 345, 1770 NE Stadium Way, Pullman, WA, 99164, USA.

E-mail: anjali.sharma@wsu.edu, k.hayashi@wsu.edu

Abstract

Endometriosis is a chronic, non-curable disease. Due to the limitations in efficacy, high recurrence rates, and untoward side effects of current treatments, the development of new, non-hormonal, targeted therapies is urgently needed. We have previously reported that niclosamide, an FDA-approved anthelmintic drug, attenuates endometriotic lesion growth. We further identified that folate receptor-β (FRβ)-positive macrophages contribute to disease progression. Significantly, niclosamide inhibits FRβ$^+$ macrophages and reduces inflammation, innervation, and angiogenesis. To develop niclosamide as a non-hormonal and immune cell-targeted therapy for endometriosis, we engineered a folic acid-conjugated 2-deoxyglucose dendrimer (FA-2DG-D) using click chemistry to enable selective FRβ-mediated uptake. Conjugation of niclosamide to FA-2DG-D yielded a targeted nanotherapeutic (FA-2DG-D-Niclo) with enhanced aqueous solubility, controlled intracellular release, and excellent batch-to-batch reproducibility. In a mouse model of endometriosis, FA-2DG-D demonstrated lesion-specific accumulation and selective internalization by FRβ$^+$ macrophages with minimal off-target organ retention. A single intraperitoneal dose of FA-2DG-D-Niclo (25 or 50 mg/kg/b.w of niclosamide) significantly reduced FRβ$^+$ macrophage burden, suppressed lesion number and volume, and markedly improved endometriosis-associated hyperalgesia at two weeks post-treatment. Together, these findings establish FRβ$^+$ macrophages as a potential target in endometriosis and present FA-2DG-D-Niclo as a non-hormonal, macrophage-focused nanomedicine for precise and effective treatment of endometriosis.

Keywords: endometriosis, niclosamide, dendrimer, macrophages, non-hormonal therapy

Graphic Abstract

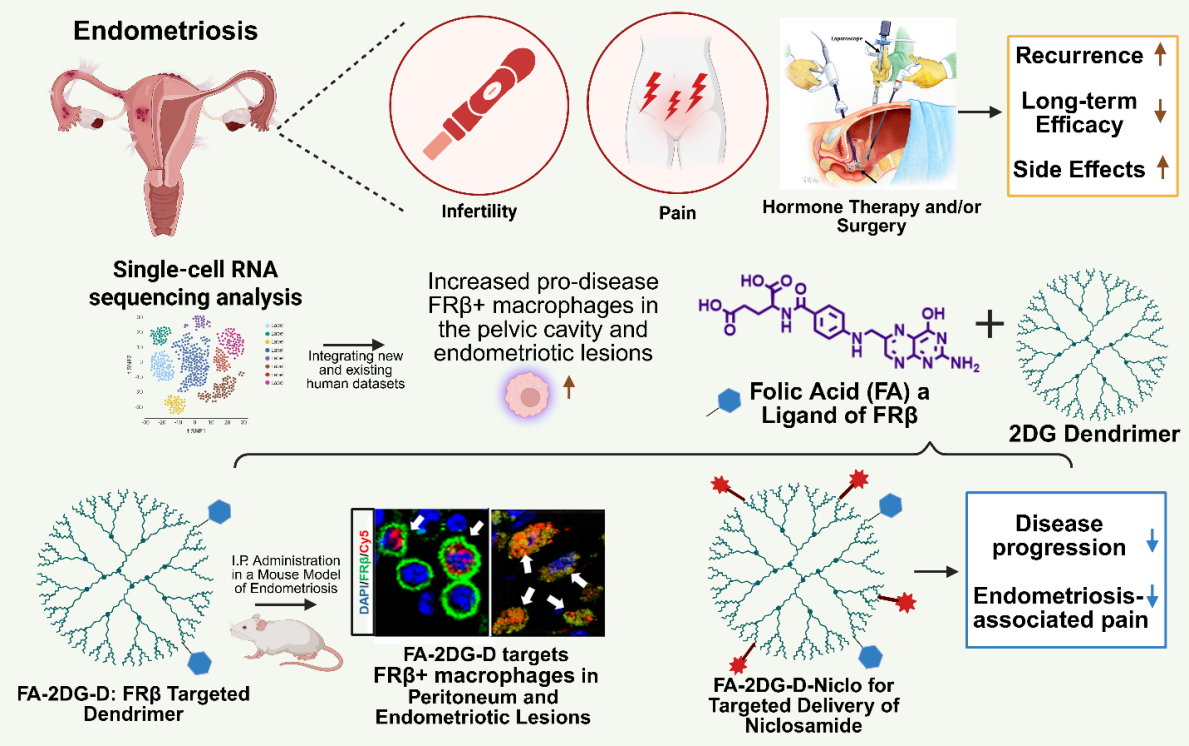

Created via Biorender.com

1. Introduction

Endometriosis affects an estimated 10% of reproductive-aged women, roughly 190 million individuals worldwide, and remains one of the most debilitating gynecological disorders.[1] The disease is characterized by chronic pelvic pain, dysmenorrhea, dyspareunia, and infertility, all of which severely diminish the quality of life for patients and their families.[2-4] In the United States alone, the annual economic burden is estimated at $78-119 billion, encompassing healthcare costs, productivity losses, and reduced workforce participation.[5] Despite its prevalence and impact, endometriosis remains incurable, and the therapeutic landscape has changed little over the past several decades. Current medical management relies on hormonal suppression of estrogen production or action,[6-7] such as oral contraceptives, progestins, and/or gonadotropin-releasing hormone (GnRH) agonists/antagonists,[6, 8], as well as surgical excision of lesions. However, hormonal treatments are limited in efficacy, have high recurrence rates, and cause significant side effects. Surgical excision offers temporary relief of symptoms, yet nearly half of surgically treated women experience recurrence within five years, and ~12% fail to achieve meaningful pain reduction after surgery.[9-10] Thus, there is an urgent need to identify new therapeutic targets to develop novel non-hormonal treatments in endometriosis.

A growing body of evidence implicates immune dysfunction, particularly macrophage dysregulation, in driving lesion establishment, chronic inflammation, angiogenesis, and neurogenesis in endometriosis.[11-13] Recently, our single-cell transcriptomic analysis identified a unique FRβ-expressing macrophage population, differentiated from monocyte-derived proinflammatory macrophages and characterized by residential macrophage traits in mouse endometriosis.[14] The population of macrophages is also identified in the lesions of endometriosis patients.[15] The selective upregulation of $FR\beta^+$ on these macrophages can be used as an accessible and disease-restricted cellular target for ligand-guided targeted drug delivery.

Our prior studies demonstrated that niclosamide significantly suppressed endometriotic lesion growth, alleviated aberrant peritoneal inflammation, and decreased vascularization and innervation in lesions using two distinct mouse models of endometriosis without compromising fertility.[11-13,16] Niclosamide is an FDA-approved anthelmintic drug with multiple clinical trials ongoing to repurpose it for the treatment of other diseases, including cancer and metabolic diseases.[17] However, the clinical use of niclosamide is significantly limited by its extremely poor aqueous solubility and correspondingly low oral bioavailability. To address these challenges,

researchers are actively developing innovative formulation strategies such as water-soluble derivatives, solid dispersions, and nanocarrier-based delivery systems to enhance its solubility, pharmacokinetic profile, and overall therapeutic potential.[18] Additionally, systemic niclosamide treatment inhibits several pathways, including STAT3, NFκB, and WNT signaling, across all cell types,[13,16], including other macrophages[14]. Disrupting these essential pathways across all cell types would lead to unwanted side effects and pose a significant barrier to developing a new therapy. Importantly, niclosamide can also reduce elevated FRβ$^+$ macrophages and restore the perturbed microenvironment in endometriosis by finely regulating macrophage dynamics[14], suggesting that FRβ$^+$ macrophages can serve as a viable therapeutic target in endometriosis. Therefore, targeted delivery of niclosamide to FRβ$^+$ macrophages offers a strategy to maximize therapeutic efficacy while minimizing systemic toxicity.

In this context, dendrimer nanotechnology has emerged as a powerful tool for targeted therapeutic delivery, enabling selective engagement of pathogenic cells while minimizing off-target toxicity.[19-24] Dendrimers are monodisperse, highly branched macromolecules whose multivalent surface architecture and tunable chemistry allow precise conjugation of targeting ligands, therapeutic agents, and imaging probes.[25-27] Building on our previously synthesized 2-deoxy-glucose (2DG) functionalized dendrimer (2DG-D),[28] which incorporates 2DG moieties to enhance solubility and macrophage interaction, we engineered a folic acid (FA), a ligand of FRβ, conjugated dendrimer (FA-2DG-D) by covalently coupling FA to the dendrimer surface through orthogonal click chemistry. This design exploits ligand-FRβ binding to selectively direct dendrimer uptake into FRβ$^+$ macrophages within endometriotic lesions and peritoneum.[29-30] To achieve targeted delivery, we further developed the niclosamide conjugated FA-2DG-D (FA-2DG-D-Niclo). Here, we report the design, synthesis, and *in vivo* evaluation of FA-2DG-D and FA-2DG-D-Niclo in a mouse model of endometriosis. Our results demonstrate that FA-2DG-D has FRβ$^+$ macrophage-specific targeting in the lesions and peritoneum and delivers niclosamide into FRβ$^+$ macrophages with ligand-receptor internalization. This targeted dendrimer platform offers a promising strategy for therapeutic delivery in endometriosis, addressing a critical unmet need for more precise and effective interventions.

2. Methods

2.1. Human Sample Collection

112 All procedures involving human subjects were performed in accordance with ethical
113 approval by the Institutional Review Board (IRB) guidelines for the University of Florida under
114 IRB code NO. IRB202003131. All patients were recruited from the Division of Minimally Invasive
115 Gynecologic Surgery of the University of Florida Health Shands Hospital, Gainesville, Florida.
116 Participants were either previously diagnosed with endometriosis or suspected of having
117 endometriosis, with symptoms including ovarian cysts, chronic pelvic pain, dysmenorrhea,
118 dyschezia, dyspareunia, uterine bleeding, and myofascial pain syndrome. Endometriosis is further
119 confirmed by pathological analysis of the excised lesions obtained during surgery. Informed
120 written consent was obtained from each participant before the procedure. In this study, peritoneal
121 washings from 4 patients aged 19 to 37 years (**Supplementary Table S1**) were collected at the
122 beginning of the procedure. Briefly, the pelvic cavity was irrigated using approximately 100 mL
123 of sterile saline, and approximately 80 mL of peritoneal washings containing pelvic exudate cells
124 were collected from each patient and placed on ice immediately. Red blood cells were removed by
125 resuspending cells with 500 µL Red Blood Cell Lysis Buffer (BioLegend, Cat.#420301). Cells
126 were then counted and cryopreserved with freezing media containing 90% fetal bovine serum
127 (FBS) and 10% dimethyl sulfoxide, and stored at −80 °C for further analysis.
128
129 ***2.2. Single-cell RNA-Sequencing and Analysis.***
130 ***2.2.1. Library Preparation and Sequencing***
131 To perform single-cell RNA sequencing (scRNA-seq), frozen pelvic exudate cells were
132 thawed in a 37 °C water bath and prepared following the 10x Genomics protocol named "Fresh
133 frozen human peripheral blood mononuclear cells for single-cell RNA sequencing" (document
134 #CG00039 Rev E). Briefly, thawed cells were slowly transferred into a 50 mL conical tube and
135 recovered by sequential 1:1 dilution with warmed FBS for a total of 5 times. Cell viability was
136 assessed to ensure samples with viability greater than 80%. After centrifuging at 300g for 5 min
137 at RT, the cells were resuspended in phosphate-buffered saline (PBS) with 0.04% bovine serum
138 albumin (BSA) at a concentration of 900-1,200 cells/µl. Cells were then placed on ice and
139 immediately proceeded to library construction using a 10x Genomics Chromium Next GEM
140 Single Cell 3' Kit v3.1, following the standard kit user guide (document #CG000204) for a target
141 of 6000 cells. Libraries were sequenced on Illumina NovaSeq 6000. FASTQ files were aligned to

142 the human reference genome GRCh38 via Cell Ranger v7.1.0,[31] and an average of 107,903 reads
143 per cell was achieved for each RNA library (**Supplementary Table S2**).
144
145 ***2.2.2. External Human Endometrial and Pelvic Exudate Cell scRNA-seq Datasets***
146 We integrated publicly available human scRNA-seq datasets from eutopic endometrium
147 with or without endometriosis, ectopic endometrium, and pelvic exudate cells. Processed Cell
148 Ranger output files or raw FASTQ files were downloaded from the Gene Expression Omnibus
149 (GEO), ArrayExpress, or the Sequence Read Archive (SRA). These datasets included: (1) Wang et
150 al. (GSE111976),[32] (2) Lai et al. (GSE183837),[33] (3) Garcia-Alonso et al. (E-MTAB-10287),[34] (4)
151 Tan et al. (GSE179640),[15] (5) Fonseca et al. (GSE213216),[35] (6) Huang et al. (GSE214411),[36] (7)
152 Marečková et al. (E-MTAB-14039),[37] (8) Shin et al. (PRJNA932195),[38] (9) Han et al.
153 (GSE228030),[39] and (10) Zou et al. (PRJNA713993),[40] as shown in **Figure 1A and B**. For all
154 datasets, only samples collected from women of reproductive age were included. For endometrial
155 scRNA-seq datasets from (1) to (8), patients labeled as undergoing hormonal treatments during
156 sample collection were also excluded. Samples used in this study are summarized in
157 **Supplementary Table S3**.
158
159 ***2.2.3. Single-cell Data Pre-processing and Clustering***
160 RNA matrices from both newly generated and existing public datasets were individually
161 imported to Scanpy v.1.8.1 for further analysis.[41] Low-quality cells were excluded using the
162 following criteria: (1) genes that were detected in fewer than 3 cells, (2) cells with fewer than 300
163 genes, (3) a maximum of 100,000 UMIs, and (4) a maximum of 20% mitochondrial content.
164 Doublets were detected and removed using Scrublet.[42] Filtered matrices from endometrial or pelvic
165 cell scRNA-seq datasets were combined separately and analyzed independently. For each
166 combined endometrial or pelvic cell scRNA-seq matrix, gene expression values were normalized
167 with a global scaling factor of 10, 000 and log-transformed. Top 3,000, or 2,000 highly variable
168 genes for the endometrial, or pelvic cell datasets, respectively, were identified by Scanpy. The
169 mitochondrial genes, haemoglobin genes, and ribosomal genes were excluded from the highly
170 variable gene set.[43] Principal component analysis (PCA) was performed using the highly variable
171 gene set. After Harmony (v.0.0.10)[44] batch effect correction, harmony-corrected components were
172 used to generate the neighborhood graph and perform dimensionality reduction using uniform

173 manifold approximation and projection (UMAP). The Leiden algorithm was then used for
174 clustering analysis.[45] Marker genes of each cluster were identified using the Wilcoxon rank-sum
175 test[46] with the default setting (**Supplementary Table S4**). Major cell types were determined by
176 manually annotating cell clusters with previously established marker genes from the literature.[15,
177 39, 47-48]
178
179 ***2.2.4. Identification of Enriched Genes and Gene Ontology Analysis in FOLR2$^+$ Endometrial***
180 ***and Pelvic Cells***
181 To understand the transcriptional profiles of FOLR2+ macrophages, cells with specific
182 FOLR2 expression (FOLR2>0) were labeled and extracted from endometrial and pelvic cell
183 matrices. Enriched genes in FOLR2$^+$ cells were identified by the Wilcoxon rank-sum test in a one-
184 versus-rest fashion, with a minimum $\log_2$(foldchange) of 2 (**Supplementary Table S5**). Gene
185 Ontology (GO) biological process was performed on the identified enriched genes in FOLR2+
186 endometrial or pelvic cells using clusterProfiler (v.4.2.2).[49] The enriched GO list was further
187 filtered with *simplify* function (cutoff = 0.7) to remove redundant terms (**Supplementary Table**
188 **S6**). Differentially expressed genes (DEGs) among eutopic endometrium without (Cont) or with
189 endometriosis (EuE), and ectopic endometrium (EcE) in the endometrial FOLR2$^+$ macrophages,
190 and DEGs between control (Cont) and endometriotic (Endo) pelvic exudate cells, were identified
191 by Wilcoxon rank-sum test, with a minimum $\log_2$(foldchange) of 0.5 (**Supplementary Table S7**).
192
193 ***2.3. Chemistry Experimental Section***
194 Experimental methods related to materials, instrumentation, synthesis protocols, *in*
195 *vitro* drug release studies, and FA-2DG-D-Niclo formulation stability studies are presented in the
196 **Supplementary Information**.
197
198 ***2.4. Animals***
199 C57BL/6 mice were purchased from Inotiv and housed in an environment-controlled
200 animal facility (20-22 °C, ~40% relative humidity, and 12:12 light-dark cycle) with ad libitum
201 access to food and water. All animal experiments were conducted at Washington State University
202 in accordance with the NIH guidelines for the care and use of laboratory animals (protocol #6751).
203

2.5. Mouse Model of Endometriosis

An experimental mouse model of endometriosis was employed, using procedures previously described and adopted by us, with minor modifications.[50] Briefly, to induce endometriosis-like lesions (ELL), female donor mice were injected subcutaneously with pregnant mare serum gonadotropin (PMSG; 5 IU; Sigma, St. Louis, MO) to stimulate an estrogenic response within the uterus. Uteri were harvested from these donors 41 hours after PMSG injection. The endometrium was then scraped from myometrium and dissected into fragments (1-2 mm per side), and introduced as the source of syngeneic mouse endometrium (50 mg of fragments) via injection (in 0.2 mL of PBS) into the peritoneal cavity in the ovary-intact recipient females under anesthesia via inhaled isoflurane.

2.6. Animal Study Design

2.6.1. In Vivo Dendrimer Biodistribution

Adult female mice (n=36, ~3 months old) were randomly divided into three groups (n=3/group/timepoint): 1) sham controls administered with Cy5-labeled dendrimer FA-2DG-D-Cy5; 2) ELL-induced mice administered with 2DG-D-Cy5; 3) ELL-induced mice administered with FA-2DG-D-Cy5. The animals in the ELL groups received donor endometrium to induce endometriotic lesions, and the sham control mice received PBS. One week following lesion induction, all mice received FA-2DG-D-Cy5 or 2DG-D-Cy5 from the tail vein, as listed in the above group description, at a dose of 50 mg/kg (300 µL). Mice were then euthanized at 1, 6, 24, and 72 hours after injection. The whole skin was gently peeled off to acquire the whole-body Cy5 fluorescence distribution using an in vivo imaging system (IVIS; Revvity). Lesions and/or major organs, including the brain, heart, spleen, lungs, liver, and kidneys, were dissected to obtain ex vivo fluorescence images and stored at -80 °C. The fluorescence intensity of the region of interest (ROI) was calculated by the Living Image software (4.7.4) accompanying IVIS. The amounts of dendrimer in major organs and lesions were further examined ex vivo using fluorescence intensity-based quantification.

2.6.2. Ex Vivo Dendrimer Quantification

Frozen organs (lesions, liver, spleen, heart, kidneys, brain, and lungs) were slowly thawed on ice and weighed. Tissue samples were then dissected to obtain known masses from each organ.

235 Samples were homogenized in methanol (1 mL per 100 mg tissue) with stainless steel beads using
236 a tissue homogenizer. The homogenized samples were centrifuged at 4 °C, and the clear
237 supernatants were transferred to protein LoBind Eppendorf tubes and stored at -80 °C. For
238 fluorescence quantification, thawed supernatants were centrifuged again before analysis.
239 Fluorescence intensity was measured on a Varioskan Lux Multimode Microplate Reader
240 (ThermoFisher), using λ_ex = 650 nm and λ_em = 670 nm for Cy5. Background fluorescence from
241 control solvent was subtracted, and the corrected fluorescence values were converted to 2DG-D-
242 Cy5 and FA-2DG-D-Cy5 concentrations using calibration curves generated at 5-10 slit widths.
243

244 ***2.6.3. In Vivo Cellular Uptake of Dendrimer***

245 To evaluate the specificity of cellular uptake of the dendrimer, 6 female mice were induced
246 with endometriosis lesions. On Day 7 following lesion induction, mice received an intraperitoneal
247 (i.p.) injection of FA-2DG-D-Cy5 or 2DG-D-Cy5 (50 mg/kg/b.w., n=3/group). Peritoneal cells,
248 lesions, kidney, liver, and spleen were collected at 2 weeks after dendrimer injection. The specific
249 cellular uptake of the dendrimer was then assessed by immunostaining.
250

251 ***2.6.4. In Vivo Efficacy of Dendrimer-Niclosamide***

252 The efficacy of targeted delivery of niclosamide with FA-conjugated dendrimer (FA-2DG-
253 D-Niclo) was examined using a mouse model of endometriosis described above. As shown in
254 **Figure 8A**. On Day 7, ELL-induced mice were administered a single i.p. injection of control (FA-
255 2DG-D), or 25 mg or 50 mg/kg body weight (b.w.) of FA-2DG-D-Niclo. Behavioral tests were
256 performed on Day -1 (a day before lesion induction), Day 7 (before dosing), and Day 14 or 21 (1
257 or 2 weeks after dosing, n=16 at Day -1 and Day 7, n=8 at Day 14 and Day 21). Mice were then
258 euthanized on Day 14 or 21 after the last behavioral test. Peritoneal fluid was recovered by lavage
259 (4 mL x 2 of ice-cold PBS with 3% FBS) for immune profiling. The number and volume of lesions
260 were recorded. Lesions were fixed in 4% paraformaldehyde for further analysis.
261

262 ***2.7. von Frey Test***

263 A standard behavioral (mechanical sensitivity) test was performed before sample
264 collection, as described by our laboratory previously.[51-52] Mice (n=8/group/time point) were
265 allowed to acclimate quietly in the testing room for 30 minutesunder red light. Then, von Frey

266 filaments (BIO-VF-M, Bioseb) were applied 10 times to the skin perpendicular to the lower
267 abdomen and bilateral hind paws to evaluate local or systemic sensitivity, respectively. The force
268 in grams (g) of the filament evoking a withdrawal response (50% response count as sensitive) was
269 recorded. Three behaviors were considered positive responses to filament stimulation: 1) sharp
270 retraction of the abdomen, 2) immediate licking and/or scratching of the area of filament
271 stimulation, or 3) jumping. All behavioral tests were performed with investigators blinded to
272 treatment groups. These data were then subsequently analyzed by another blinded investigator.
273
274 ***2.8. Flow Cytometry***
275 Single-cell suspensions of peritoneal exudate cells were used for immune cell profiling by
276 flow cytometry as described previously.[51-52] Briefly, peritoneal exudate cells were lysed using Red
277 Blood Cell Lysis Buffer (BioLegend) and incubated at room temperature for 20 minuteswith
278 Zombie Aqua™ Fixable Viability dye (BioLegend). The cells were blocked on ice for 20
279 minuteswith Fc Block anti-CD16/CD32 (ThermoFisher) and stained with fluorochrome-
280 conjugated monoclonal antibodies for 1 hour (**Supplementary Table S8**). Samples (n=8/group)
281 were acquired with the Attune NxT Acoustic Focusing Cytometer using Attune NxT software
282 (ThermoFisher), and data were analyzed with FlowJo v10.4 software (FLOWJO).
283
284 ***2.9. Immunohistochemistry and Confocal Imaging***
285 The peritoneal exudate cell suspension was first fixed with 4% paraformaldehyde at RT for
286 15 min, and blocked with 10% donkey serum at RT for 30 min. The cells were then incubated with
287 FRβ primary antibody (1:200, Abcam, Cat.#ab302532) at 4 °C overnight and AlexaFluor 488-
288 conjugated F(ab') secondary antibody (Molecular Probe) at RT for 1 hour. Following DAPI
289 staining, the cells were resuspended with Fluoromount-G (SouthernBiotech) and mounted on
290 slides. The mounted slides were imaged using a Leica SP8-X Confocal Microscope.
291 Immunohistochemistry of FRβ on cross-sections (5 μm) of paraffin-embedded tissues,
292 including lesion, kidney, and liver, was performed using the FRβ primary antibody (1:400) and
293 AlexaFluor 488-conjugated F(ab') secondary antibody, or VECTASTAIN ABC kit (Vector Lab).
294 Immunostaining images were acquired by Leica SP8-X Confocal Microscope or Leica DM4 B
295 microscopy. FRβ-positive cells in lesions were counted by Image J in an area of 0.07244 mm^2, and
296 the number of $FR\beta^+$ cells per 1 mm^2 was shown.

297

298 ***2.10. Statistical Analysis***

299 Statistical analyses were performed using GraphPad Prism (version 9.5). To compare
300 differences in dendrimer organ uptake among groups, one-way ANOVA followed by Tukey's
301 multiple comparison tests was used. To analyze the behavioral test results, time-dependent
302 differences within a single group were compared using a one-way ANOVA followed by Dunnett's
303 multiple-comparison test. To compare the effects of different dosages of niclosamide at each time
304 point, one-way ANOVA was used with Tukey's multiple comparison tests. Differences in lesion
305 number, volume, and FRβ$^+$ or CD45$^+$ cell counts between groups at each time point were analyzed
306 using one-way ANOVA followed by Tukey's multiple-comparison test. In all cases, data were
307 tested for normal distribution using the Shapiro-Wilk normality test. If data were normally
308 distributed, one-way ANOVA was used to analyze differences among groups. If data were not
309 normally distributed, the Kruskal-Wallis test was performed, as stated in the figure caption.
310 Significance was defined as $p < 0.05$ (*), $p < 0.01$ (**), $p < 0.001$ (***), or $p < 0.0001$ (****).

311

312 **3. Results and Discussion**

313 ***3.1. FRβ-expressing Macrophages in Eutopic and Ectopic Endometrium, and Pelvic Exudate***
314 ***Cells in Endometriosis***

315 We performed an integrated analysis with our newly generated pelvic exudate cell scRNA-
316 seq dataset from women with endometriosis (**Supplementary Tables S1 and S2**), along with
317 publicly available human datasets, including eutopic endometrium without or with endometriosis,
318 ectopic endometrium (lesion), and pelvic exudate cells (**Figure 1A-B, Supplementary Table S3**).
319 After data merging and quality control filtering, 748,509, and 76,187 total high-quality endometrial
320 and pelvic exudate cells were retained, respectively. Clustering analysis identified 7 major cell
321 types in the endometrium (EM), including B lymphocytes (CD79A$^+$), endothelial cells
322 (PECAM1$^+$), epithelial cells (EPCAM$^+$), myeloid cells (LYZ$^+$), perivascular cells (RGS5$^+$),
323 stromal cells (DCN$^+$), and T lymphocytes and natural killer (NK) cells (CD3E$^+$ and CD2$^+$) (**Figure**
324 **1C and E, Supplementary Table S4**). In the pelvic cavity (P), B lymphocytes (CD79A$^+$),
325 dendritic cells (CD1C$^+$), macrophages (Mac, CD14$^+$), mast cells (TPSAB1$^+$), NK cells (GNLY$^+$),
326 and T lymphocytes (CD3D$^+$) were assigned as overarching cell types (**Figure 1D and F,**
327 **Supplementary Table S4**). As expected, UMAP projection confirmed that FOLR2$^+$ cells are

328 localized within the myeloid cell clusters of endometrial and pelvic exudate cells (**Figure 1G-H**).
329 Gene Ontology (GO) enrichment analysis indicated that both endometrial and pelvic FOLR2$^+$
330 macrophages were primarily associated with myeloid migration and activation, and immune
331 regulation (**Figure 1I-J, Supplementary Table S6**). In particular, biological processes associated
332 with cytokine production, leukocyte cell-cell adhesion, and interleukin-6 (IL6) production were
333 predominantly enriched in the FOLR2$^+$ macrophages of the endometrium. Stronger association
334 with phagocytosis, cholesterol regulation, and response to bacteria was detected in the pelvic
335 FOLR2$^+$ macrophages, consistent with the primary roles of residential FOLR2$^+$ macrophages in
336 host defense and metabolic processes.[53-55] Comparative analysis showed a significantly higher
337 abundance of FOLR2$^+$ macrophages in the ectopic endometrium (EcE) than those in the eutopic
338 endometrium with (EuE) and without (Cont) endometriosis (**Figure 1K**). Similarly, in pelvic
339 exudate cells, significantly elevated FOLR2$^+$ macrophages were observed in patients with
340 endometriosis (**Figure 1L**). Furthermore, differential gene expression (DEG) analysis of
341 endometrial and pelvic FOLR2$^+$ macrophages demonstrated that significant upregulation of
342 proinflammatory (CCL2, IL6R, and NFKB1), angiogenesis (FGFR1, HIF1A, and MMP2), and
343 adhesion-related genes (ITGAV, TGFBR1, and TGFBR2) in endometriosis-associated
344 endometrium (EuE and/or EcE) and pelvic cells (Endo) (**Figure 1M-N, Supplementary Table**
345 **S7**). Collectively, these results indicate an expansion of a pro-disease FOLR2$^+$ macrophage
346 subpopulation in the ectopic endometrium and pelvic cavity in endometriosis patients with pro-
347 disease functions.
348
349 ***3.2. Synthesis and Characterization of FA-2DG-D Using Click Chemistry***
350 A major challenge in developing nanomaterial-based drug delivery systems lies in the
351 complexity and limited reproducibility of synthetic procedures, scalability constraints, and poor
352 batch-to-batch consistency. To overcome these limitations, we designed and synthesized the FA-
353 2DG-D conjugate capable of selectively targeting FRβ$^+$ macrophages for treating endometriosis
354 using an efficient copper(I) catalyzed alkyne-azide cycloaddition (CuAAC) click reaction. This
355 click chemistry-based approach offers a robust and versatile strategy for achieving precise,
356 reproducible, and site-specific conjugation of targeting ligands or therapeutic molecules to
357 polymeric nanocarriers, including dendrimers.[28, 56-58]

358 Folic acid (**1**) was functionalized with an azide group to enable its participation in the
359 CuAAC reaction. The folate receptor recognizes folic acid through its pterin and p-aminobenzoate
360 moieties via multiple hydrogen bonds and electrostatic interactions within the receptor pocket.[59]
361 To preserve these recognition elements, conjugation with the azide linker was performed through
362 the α-carboxylic acid group of the glutamic acid residue, forming a stable amide linkage with the
363 terminal amine of the linker. The carboxylic acid in the ligand was activated using
364 dicyclohexylcarbodiimide (DCC) and *N*-Hydroxysuccinimide (NHS), and the resulting NHS-
365 activated intermediate was reacted with azido-PEG5-amine (**2**) in the presence of DIPEA to yield
366 the desired FA-Azide (**3**). Successful formation of the azide-functionalized folic acid was
367 confirmed by ^{1}H NMR spectroscopy, which showed characteristic PEG proton signals from the
368 azide linker at δ 3.0 (2H), 3.4 (2H), and 3.5-3.7 (20H) ppm, along with a new amide proton signal
369 at δ 7.3 ppm (**Figures 2B and S1**). HPLC analysis confirmed the purity of the product, exhibiting
370 a single peak with a retention time of 13.3 minutes with more than 98% purity (**Figure S3**). To
371 enable the subsequent CuAAC coupling, terminal alkyne groups were introduced on the surface
372 of 2DG-D. The primary hydroxyl groups of the surface-exposed 2DG moieties were utilized for
373 this modification. 2DG-D (**4**) was reacted with 5-hexynoic acid (**5**) in the presence of EDC and
374 DMAP to afford 2DG-D-Hexyne (**6**) (**Figure 2A**). ^{1}H NMR spectrum showed new methylene
375 proton signals from the hexynoic linker in the aliphatic region at δ 1.75-1.68 (8H), 2.46–2.34, and
376 2.74-2.58 (8H) ppm (**Figures 2B and S5**) confirming the attachment of 4 hexyne arms. HPLC
377 analysis showed a shift in retention time from 14.0 minutes for 2DG-D (**4**) to 19.7 minutes for
378 2DG-D-Hexyne (**6**), confirming successful surface modification (**Figures S7 and S15**). Finally,
379 the CuAAC reaction between FA-Azide (**3**) and 2DG-D-Hexyne (**6**) yielded the FRβ^{+} macrophage-
380 targeted platform FA-2DG-D (**7**). Previous studies have demonstrated that dendrimers bearing a
381 single folic acid ligand exhibit monovalent, reversible binding with folate-binding protein (FBP),
382 whereas dendrimers conjugated with two or more folic acid molecules engage in multivalent
383 interactions, resulting in stronger receptor binding.[60-62] Given the high hydrophobicity of folic acid,
384 conjugating more than 2 ligand molecules could potentially reduce the dendrimer's aqueous
385 solubility. Our CuAAC click chemistry approach ensured desired loading of folic acid on the
386 dendrimer. The number of attached molecules was confirmed through the comparative integration
387 of aromatic protons from the dendrimer at δ7.2 ppm (16H), and the aromatic and amide protons of
388 folic acid at δ8.7 ppm (2H), 7.7 ppm (4H), 7.0 ppm (4H) and at 6.7 ppm (4H). The HPLC

chromatogram showed a retention time shift from 19.7 minutes for 2DG-D-Hexyne (**6**) to 16.1 minutes for FA-2DG-D (**7**). The purity of FA-2DG-D (**7**) was determined to be more than 96% by HPLC (**Figures S10 and S15**). Dynamic light scattering (DLS) analysis revealed a hydrodynamic diameter of 6.6 ± 0.4 nm and a zeta potential of –5.8 ± 0.3 mV (**Figures S11 and S12**).

To enable visualization and assessment of uptake of the dendrimer in FRβ$^+$ macrophages in endometriosis, the dendrimer was further functionalized with a near-infrared dye, cyanine 5 (Cy5). The FA-2DG-D **(7)** containing approximately two terminal alkynes on its surface was conjugated with Cy5-azide (**8**) via a CuAAC reaction, yielding the fluorescently labeled FA-2DG-D-Cy5 (**9**). Successful conjugation was confirmed by the appearance of characteristic Cy5 proton signals in the ^{1}H NMR spectrum (**Figure 2B**). The number of Cy5 molecules attached to the dendrimer surface was estimated by proton integration. Comparison of the dendrimer aromatic protons at δ 7.2 ppm (16H) with the Cy5 aromatic protons at δ 8.4 (4H), 8.2 (4H), 7.4 (4H), 6.6 (2H), and 6.4 ppm (2H) indicated the attachment of approximately two Cy5 molecules (**Figures 2B and S13**). The HPLC chromatogram of FA-2DG-D-Cy5 (**9**) exhibited a retention time shift from 16.1 to 17.7 minutes following Cy5 conjugation, with a purity exceeding 97% (**Figures S14 and S15**). In addition, the Cy5-labeled dendrimer displayed a characteristic UV absorbance at 650 nm, corresponding to Cy5, which further confirmed successful conjugation. A Cy5-labeled 2DG-D dendrimer (2DG-D-Cy5), lacking the folic acid targeting ligand, was prepared as a non-targeted control for uptake studies following our previously reported procedure.[27]

3.3. Fluorescence Imaging and Quantitative Analysis of the Biodistribution of Systemically Administered 2DG-D-Cy5 and FA-2DG-D-Cy5 in a Mouse Model of Endometriosis

We first evaluated the selective FRβ$^+$ macrophages targeting capability of FA-2DG-D-Cy5 in ELL-induced mice at 1, 6, 24, and 72 hours (n=3) and compared it with sham controls (n=3). To evaluate the contribution of folic acid (FA) toward lesion targeting, biodistribution studies of non-targeted 2DG-D-Cy5 in ELL-induced mice (n=3) were also performed under identical conditions (**Figure 3**). One week after lesion induction, 50 mg/kg b.w. of fluorescently labeled (FA-2DG-D-Cy5) or non-targeted (2DG-D-Cy5) was injected into the tail vein. Cy5 fluorescent signals were calculated via the IVIS system at 1, 6, 24, and 72 hours. FRβ$^+$ macrophages in the lesions showed a pronounced elevation in fluorescent (Cy5) signal starting at 1 hour post-injection (green arrows), which persisted above that of the 2DG-D-Cy5 group over the

420 72-hour observation period (**Figure 3A**). The *ex vivo* fluorescent results at 72 hours showed
421 specific uptake of FA-2DG-D-Cy5 in the lesion, although some nonspecific uptake of FA-2DG-
422 D-Cy5 and 2DG-D-Cy5 was observed primarily in the liver and kidneys (**Figure 3B-C**). For more
423 precise quantification, frozen tissue samples from the 1, 6, 24, and 72-hour groups were
424 homogenized, and fluorescence intensity was measured to assess quantitative dendrimer uptake in
425 lesions and major organs. Both FA-2DG-D-Cy5 and 2DG-D-Cy5 showed strong, persistent
426 accumulation within endometriosis lesions beginning at 1-hour post-injection and sustained
427 through 72 hours **(Figures 3D and S16)**. By 72 hours, lesion uptake of FA-2DG-D-Cy5 was
428 significantly higher than that of 2DG-D-Cy5, suggesting its targeted accumulation in FRβ$^+$
429 macrophages that are abundant in endometriotic lesions. (**Figure 3D-E and Figure S16**).
430 Moreover, FA-2DG-D-Cy5 demonstrated minimal accumulation (<5% Injected Dose (%ID)) in
431 other major organs, indicating rapid clearance from off-target tissues **(Figure 3E)**. Importantly,
432 unlike many nanoparticle systems that exhibit up to ~80% hepatic accumulation, FA-2DG-D-Cy5
433 showed only ~4% liver accumulation, comparable to the previously characterized 2DG-D-Cy5
434 platform, demonstrating its favorable pharmacokinetic profile.[27]
435
436 ***3.4. Confocal Imaging of Cellular Uptake of Intraperitoneally Administered FA-2DG-D-Cy5***
437 ***and 2DG-D-Cy5 in a Mouse Model of Endometriosis***
438 We next examined the targeting ability, including selective cellular uptake, localization,
439 and retention of FA-2DG-D-Cy5 or 2DG-D-Cy5 in ELL-induced mice 2 weeks after dendrimer
440 administration (**Figure 4**). Confocal imaging showed that FA-2DGD-Cy5 (red) was selectively
441 targeted and taken up by FRβ$^+$ macrophages (green), not only in lesions but also in peritoneal
442 exudate cells (**Figure 4A-B, white arrows**), where FRβ$^+$ macrophages were elevated in ELL-
443 induced mice. In contrast, cellular uptake of 2DG-D-Cy5 without FA ligand was limited in the
444 lesion and peritoneal cells (**Figure 4A-B**). Given the potential uptake of non-targeted 2DG-D-Cy5
445 by activated macrophages,[28] we further quantified nonspecific FA-2DG-D-Cy5 internalization in
446 peritoneal exudate cells. The uptake was an average of 0.59%, indicating negligible nonspecific
447 internalization. No dendrimer retention was observed in the kidneys, liver, or spleen in ELL-
448 induced mice 2 weeks following dendrimer administration **(Figure 4C)**, indicating that FA-2DG-
449 D-Cy5 underwent complete clearance, and off-target accumulation in major organs was negligible.
450 These results suggest that FA-2DGD-Cy5 dendrimer is internalized only by ligand-receptor

451 endocytosis in FRβ$^+$ macrophages in the lesions and peritoneal cells. As it remains stable within
452 cells for at least 2 weeks, it is an excellent nanocarrier for drug delivery.
453
454 ***3.5. Synthesis and Characterization of FA-2DG-D-Niclo Conjugate Using Click Chemistry***
455 We developed a niclosamide-labeled dendrimer platform, FA-2DG-D-Niclo, by
456 conjugating niclosamide to the FA-2DG-D, to enable targeted delivery of niclosamide to disease-
457 driving FRβ$^+$ macrophages as a therapy for endometriosis. To achieve high conjugation efficiency
458 and precise drug loading, CuAAC was employed. Accordingly, a niclosamide bearing an azide
459 linker (Niclo-Azide) was first synthesized by functionalizing the phenolic -OH group of
460 niclosamide. Several linker architectures were explored to identify a construct that combined
461 physiological stability with controlled intracellular release. Initially, aliphatic and PEG-based
462 carboxylic acids were coupled to niclosamide through EDC/DMAP-mediated esterification,
463 aiming to generate ester linkages that are labile in the intracellular conditions and stable at
464 physiological pH. However, due to the proximity of the ester group to the aromatic ring, the
465 resulting phenolic esters exhibited instability and underwent rapid cleavage during subsequent
466 CuAAC reactions.[63] To circumvent this issue, a previous report on a disulfide-linker-based
467 niclosamide prodrug was followed. We subsequently designed and synthesized niclosamide-azide
468 (niclo-azide) containing a disulfide linker.[64] It was reported that the disulfide linker remains stable
469 under extracellular conditions but undergoes selective cleavage in the intracellular environment,
470 thereby releasing free niclosamide.[64]
471 The synthesis of niclo-azide was carried out through a multistep route (**Figure 5A**). The
472 Boc-protected disulfide derivative **(10)** was synthesized using a published procedure.[64] It was then
473 deprotected using 4 N HCl in dioxane to afford compound **11** as the amine hydrochloride salt,
474 which was directly converted to the corresponding carbamoyl chloride intermediate **12** using
475 triphosgene, following coupling with niclosamide **(13)** under mild basic conditions to afford the
476 desired Niclo-Azide **(14) (Figure 5A)**. Successful formation of the product was confirmed by
477 comparative integration in ^{1}H NMR spectroscopy, which showed characteristic aromatic protons
478 from the niclosamide scaffold δ 8.4-7.3 ppm (6H) and the aliphatic protons from the disulfide
479 linker between δ 3.7-2.7 ppm (11H) **(Figures 5B and S19)**. The product purity ~ 95.9%, was
480 verified by HPLC, which showed a chromatogram with a retention time of 14.7 minutes **(Figures**
481 **6A and S21).** To enable the subsequent CuAAC coupling, 2DG-D **(4)** was partially modified with

482 5-hexynoic acid. Approximately 12 hydroxyl groups per dendrimer were modified to yield 2DG-
483 D-Hexyne' **(15) (Figure 5A)**. The formation of the required product was confirmed by the
484 appearance of characteristic methylene proton signals from the hexynoic linker in the aliphatic
485 region of the ^{1}H NMR spectrum at δ 1.7 (24H), 2.4 (24H) and at 2.2 ppm **(Figures 5B and S23)**
486 which confirmed the presence of 12 hexyne arms. HPLC analysis of 2DG-D-Hexyne' **(15)** showed
487 the chromatogram at 10.4 minutes with a purity exceeding 97% **(Figure 6A)**. Subsequently, a
488 CuAAC reaction between FA-Azide **(3)** and 2DG-D-Hexyne' **(15)** yielded FA-2DG-D' **(16)**. The
489 ^{1}H NMR spectrum of FA-2DG-D' **(16)** showed characteristic aromatic resonances corresponding
490 to folic acid, confirming successful conjugation of 2 molecules per dendrimer **(Figure S26).** The
491 resulting construct retained approximately ten free terminal alkyne groups per dendrimer. The
492 HPLC chromatogram exhibited a retention time shift from 10.4 minutes for 2DG-D-Hexyne' to
493 9.6 minutes for FA-2DG-D' **(16)**, with a purity of ~98% **(Figures 6A and S28)**. Lastly, FA-2DG-
494 D' **(16)** was conjugated with Niclo-Azide **(14)** through CuAAC to obtain FA-2DG-D-Niclo **(17)**.
495 Consistent with our previous studies, [56, 58] we aimed to maintain the drug loading between 10 and
496 15% to ensure aqueous solubility of the dendrimer conjugate. Drug loading was calculated by ^{1}H
497 NMR spectroscopy through comparison of the dendrimer aromatic protons at δ 7.2 ppm (16H)
498 with the newly aromatic signals at δ 8.4 (10H), 8.3 (10H), and 8.2-7.8 ppm, along with distinct
499 amide protons of niclosamide at δ 10.43 ppm (10H), confirmed the conjugation of approximately
500 ten niclosamide molecules per dendrimer, corresponding to ~12% drug loading by weight **(Figures**
501 **5B and S29)**. HPLC analysis revealed a shift in retention time from 9.6 minutes for FA-2DG-D'
502 **(17)** to 11.2 minutes for FA-2DG-D-Niclo **(17)**, with a final purity of more than 98% **(Figure S31)**.
503 DLS analysis indicated a hydrodynamic diameter of 7.6 ± 0.6 nm and a zeta potential of -7.7 ± 0.6
504 mV **(Figure 6C)**. While niclosamide is practically insoluble in water (~5 μg/mL),[65] the dendrimer-
505 drug conjugate exhibited excellent aqueous solubility (~150 mg/mL). At a drug loading of 12%,
506 this corresponds to an effective niclosamide solubility of approximately 18 mg/mL in water,
507 representing a ~3,600 fold increase in solubility compared to free niclosamide **(Figure 7A)**. The
508 physicochemical properties of FA-2DG-D-Niclo **(23)** are presented in **Figure 7A.**

509 The shelf stability of FA-2DG-D-Niclo **(17)** (1 mg/mL) was assessed in PBS at 4 °C, room
510 temperature (25 °C), and 40 °C over a 30-day period. The formulation remained stable throughout
511 the study, retaining more than 96% purity by HPLC at all tested temperatures **(Figure S34)**. No

512 shifts in retention time were observed over 30 days, confirming the chemical stability of the
513 formulation under these conditions.
514
515 ***3.6. Scalable and Reproducible Synthesis of FA-2DG-D-Niclo***
516 Ensuring synthetic reproducibility and scalability remains a central barrier in advancing
517 nanoparticle-based therapeutics toward clinical applications. To overcome these challenges, we
518 established a streamlined and scalable synthetic workflow for FA-2DG-D-Niclo **(17)** that enables
519 rigorous characterization of intermediates at each stage. To assess batch-to-batch consistency, three
520 independent 400 mg-scale batches were synthesized and evaluated by ^{1}H NMR and HPLC. The
521 ^{1}H NMR spectra of all three batches **(Figure 7B, left)** showed identical chemical profiles and
522 consistent drug and ligand loading. Similarly, HPLC analysis revealed overlapping chromatogram
523 peaks with retention times of ~11.2 minutes and purities exceeding 98%, confirming robust batch-
524 to-batch reproducibility **(Figure 7B, right)**.
525
526 ***3.7. In vitro drug release studies for FA-2DG-D-Niclo***
527 We further assessed the *in vitro* drug-release profile of the conjugate under conditions
528 mimicking both the extracellular environment (PBS + 0.1 mM GSH and 100% human plasma) and
529 the intracellular microenvironment (pH 5.5 citrate buffer + 10mM GSH) **(Figure 7C)**. Since
530 niclosamide is attached to the dendrimer through a disulfide linkage, it enables glutathione (GSH)
531 responsive cleavage.[66] Upon cleavage, the generated free thiol is known to undergo an
532 intramolecular nucleophilic attack on the tertiary carbamate, ultimately yielding free
533 niclosamide.[64] When conjugated to the targeted FA-2DG-D, this design facilitates controlled
534 release within the intracellular environments while limiting premature systemic exposure outside
535 the lesion sites. In PBS and 0.1mM GSH, the conjugate was found to be relatively stable. Less
536 than 40% of the drug was observed to be released in around 2 weeks, with negligible drug release
537 detected for the first 5 days. Notably less than 5% of the drug was released within 8 hours. When
538 incubated in human plasma, less than 35% of the drug was released over 120 hours, indicating
539 stability in physiological conditions **(Figure 7C).** Under intracellular conditions (pH 5.5 citrate
540 buffer + 10mM GSH), the conjugate showed a sustained release profile, with ~45% released in the
541 first 48 hours, ~80% at 48 hours, and reaching 95% over 15 days **(Figure 7C)**. The targeted and

542 sustained intracellular drug release profile is important to maintain the efficacy of the drug for a
543 long time and to avoid off-target effects.
544

545 ***3.8. FA-2DG-D-Niclo attenuates lesion progression and endometriosis-associated hyperalgesia.***

546 Lastly, we assessed the efficacy of FA-2DG-D-Niclo in endometriosis disease progression
547 and endometriosis-associated hyperalgesia. After the lesion induction, a single dose of FA-2DG-
548 D-Niclo dendrimer (25 or 50 mg/kg b.w. of niclosamide) or FA-2DG-D without niclosamide
549 control was administered i.p. in ELL-induced mice at Day 7, as shown in **Figure 8A**. Then, the
550 efficacy of dendrimers was examined 7 (Day 14) and 14 (Day 21) days after dendrimer
551 administration. We first confirmed the suppressing capability of FRβ^+ macrophages in the lesions
552 and peritoneal cavity by FA-2DG-D-Niclo dendrimer (**Figure 8B-C**). Single dosing of FA-2DG-
553 D-Niclo (50 mg/kg b.w.) significantly reduced FRβ^+ macrophages in the lesions at Day 21,
554 although the reduction of FRβ^+ macrophages was not observed at Day 14 (**Figure 8B**). Peritoneal
555 FRβ^+ macrophage population was reduced by both doses (25 and 50 mg/kg b.w.) of FA-2DG-D-
556 Niclo (**Figure 8C**). The results indicate that 7 days after dendrimer administration may not be
557 sufficient to reduce FRβ^+ macrophages in both lesions and the peritoneum. Indeed, lesion number
558 and volume were also significantly reduced at Day 21 by FA-2DG-D-Niclo at both doses, but there
559 were no significant differences in lesion number or volume at Day 14 (**Figure 9A**). However, we
560 realized that three mice treated with both doses and examined at Day 14 did not have lesions.
561 Furthermore, four and five mice, at doses of 25 and 50 mg/kg b.w. of niclosamide, respectively,
562 did not have lesions by Day 21, either. Thus, a single dose of FA-2DG-D-Niclo administration
563 completely inhibited lesion growth and progression in 37.5-62.5% of mice, whereas all control
564 mice developed lesions on Days 14 and 21. While reduced FRβ^+ macrophages in the remaining
565 lesions were observed only at Day 21, a few mice at Day 14 lacked lesions for examination,
566 suggesting that FA-2DG-D-Niclo was likely effective for lesion growth 7 days after
567 administration. In support of this implication, abdominal and hindpaw hypersensitivities were
568 already improved at Day 14 (**Figure 9B**). The sensitivity of the abdominal and hindpaw 7 days
569 after lesion induction was high compared with that at Day -1 before lesion induction. At Day 14,
570 FA-2DG-D-Niclo at a dose of 50 mg/kg b.w. of niclosamide significantly reduced the abdominal
571 sensitivity, which is considered peripheral visceral pain. Both doses of FA-2DG-D-Niclo improved
572 hindpaw sensitivity, which is likely be affected by peripheral and central sensitization. By Day 21,

573 FA-2DG-D-Niclo, with both doses, further improved abdominal and hindpaw sensitivities. The
574 results clearly showed that a single dose of FA-2DG-D-Niclo inhibited disease progression and
575 endometriosis-associated hyperalgesia. Notably, a single dose of FA-2DG-D-Niclo remained
576 effective for 2 weeks after administration. The current FDA-approved niclosamide treatment
577 requires a high dose (2g/day) due to its low water solubility and is limited to oral administration
578 for 7 days. Niclosamide treatment for patients who have endometriosis would need to be longer
579 due to the chronic nature of the disease. Long-term systemic treatment with niclosamide could
580 cause off-target actions. Therefore, the 2DG-D-based delivery of niclosamide and targeting of
581 disease-specific FRβ$^+$ macrophages is highly translational, as FA-2DG-D can deliver niclosamide
582 intracellularly into FRβ$^+$ macrophages, thereby enhancing efficacy, reducing side effects, and
583 treating chronic diseases such as endometriosis.
584
585 **4. Conclusions**
586 With integrated single-cell transcriptomic analysis, we further identified a significant
587 recruitment of pro-disease FRβ$^+$ macrophages within human endometriotic lesions and pelvic
588 cavity, mirroring our observations in the mouse model. Importantly, the overexpression of FRβ on
589 these macrophages provides a ligand-guided entry point, enabling receptor-specific targeting for
590 both imaging and therapeutic interventions. Leveraging this receptor overexpression, we
591 engineered a folic acid-conjugated dendrimer (FA-2DG-D) to exploit FRβ-mediated uptake for
592 targeted imaging and drug delivery in endometriotic lesions. FA-2DG-D offers several critical
593 advantages for translational development. The dendrimer architecture enables precise,
594 reproducible conjugation of targeting ligands and therapeutic payloads via click chemistry,
595 resulting in well-defined nanostructures, excellent aqueous solubility, and robust batch-to-batch
596 consistency. Conjugation of niclosamide to generate FA-2DG-D-Niclo markedly enhanced the
597 solubility of this poorly water-soluble drug, enabled controlled, intracellularly triggered release
598 via a disulfide linker, and minimized premature systemic exposure. Importantly, the formulation
599 demonstrated high stability under physiological and storage conditions. In a mouse model of
600 endometriosis, the Cy5-labelled platform demonstrated lesion and peritoneal cell-specific
601 accumulation and intracellular internalization along with a favorable biodistribution with minimal
602 off-target organ accumulation. FA-2DG-D-Niclo enabled targeted delivery to disease-driving
603 macrophages. Administration of FA-2DG-D-Niclo led to significant reductions in lesion number

604 and volume, and improved hyperalgesia, highlighting both therapeutic efficacy and
605 immunomodulatory activity. This work demonstrates the potential of FA-2DG-D platform to target
606 FRβ$^+$ macrophages for the treatment of endometriosis. By addressing key limitations of current
607 hormonal and systemic treatments, this approach establishes a non-hormonal, FRβ$^+$ macrophage-
608 focused strategy for the treatment of endometriosis.
609
610 **Data Availability Statement**
611 The raw data of scRNA sequencing have been deposited to NCBI/SRA
612 (PRJNA1418167). Additional data or materials related to the findings of this study are available
613 from the corresponding author upon reasonable request.
614
615 **Funding Information**
616 This work was supported by NIH/NICHD, R01HD104619 (to Kanako Hayashi),
617 Washington Research Foundation Technology Commercialization Phase 1 (Kanako Hayashi and
618 Anjali Sharma).
619
620 **Declaration of Interest Statement:**
621 The authors A.S, R.S, A.D, and A.I.D have pending patents and invention disclosures on
622 2DG dendrimers and their conjugates.
623
624 **Authorship Contribution Statement**
625 A.S. and K.H. designed the research; A.D., A.S., and R.S. designed and synthesized the
626 dendrimers; M.S., M.H., and T.P. performed the animal experiments and/or analyzed the data;
627 A.D., K.J.G., and A.I.D. performed quantitative biodistribution analysis; N.S.M., V.K.S., and
628 P.S.C. collected/or prepared the human samples; M.S. performed single-cell RNA sequencing
629 and analysis; A.D., M.S., R.S., A.S., and K.H. wrote the paper; all authors read, reviewed, edited,
630 and approved the manuscript.

References

1. Zondervan KT, Becker CM, and Missmer SA. Endometriosis. The New England journal of medicine **2020**;382(13):1244-56.
2. Burney, R. O.; Giudice, L. C., Pathogenesis and pathophysiology of endometriosis. *Fertility and sterility* **2012,** *98* (3), 511-9.
3. As-Sanie, S.; Mackenzie, S. C.; Morrison, L.; Schrepf, A.; Zondervan, K. T.; Horne, A. W.; Missmer, S. A., Endometriosis: A Review. *JAMA* **2025,** *334* (1), 64-78.
4. Giudice, L. C.; Kao, L. C., Endometriosis. *Lancet (London, England)* **2004,** *364* (9447), 1789-99.
5. Ellis, K.; Munro, D.; Clarke, J., Endometriosis Is Undervalued: A Call to Action. *Frontiers in global women's health* **2022,** *3*, 902371.
6. Marla, S.; Mortlock, S.; Heinosalo, T.; Poutanen, M.; Montgomery, G. W.; McKinnon, B. D., Gene expression profiles separate endometriosis lesion subtypes and indicate a sensitivity of endometrioma to estrogen suppressive treatments through elevated ESR2 expression. *BMC Medicine* **2023,** *21* (1), 460.
7. Edi, R.; Cheng, T., Endometriosis: Evaluation and Treatment. *American family physician* **2022,** *106* (4), 397-404.
8. Alonso, A.; Gunther, K.; Maheux-Lacroix, S.; Abbott, J., Medical management of endometriosis. *Current opinion in obstetrics & gynecology* **2024,** *36* (5), 353-361.
9. Guo, S.-W., Recurrence of endometriosis and its control. *Human Reproduction Update* **2009,** *15* (4), 441-461.
10. Singh, S. S.; Gude, K.; Perdeaux, E.; Gattrell, W. T.; Becker, C. M., Surgical Outcomes in Patients With Endometriosis: A Systematic Review. *Journal of obstetrics and gynaecology Canada : JOGC = Journal d'obstetrique et gynecologie du Canada : JOGC* **2020,** *42* (7), 881-888.e11.
11. Shi, M.; Sekulovski, N.; Whorton, A. E.; MacLean, J. A., 2nd; Greaves, E.; Hayashi, K., Efficacy of niclosamide on the intra-abdominal inflammatory environment in endometriosis. *FASEB journal : official publication of the Federation of American Societies for Experimental Biology* **2021,** *35* (5), e21584.
12. Sekulovski, N.; Whorton, A. E.; Shi, M.; MacLean, J. A., II; Hayashi, K., Endometriotic inflammatory microenvironment induced by macrophages can be targeted by niclosamide†. *Biology of reproduction* **2019,** *100* (2), 398-408.
13. Sekulovski, N.; Whorton, A. E.; Tanaka, T.; Hirota, Y.; Shi, M.; MacLean, J. A.; de Mola, J. R. L.; Groesch, K.; Diaz-Sylvester, P.; Wilson, T.; Hayashi, K., Niclosamide suppresses macrophage-induced inflammation in endometriosis†. *Biology of reproduction* **2020,** *102* (5), 1011-1019.
14. Zhao, L.; Shi, M.; Winuthayanon, S.; MacLean, J. A., 2nd; Hayashi, K., Niclosamide targets the dynamic progression of macrophages for the resolution of endometriosis in a mouse model. *Communications biology* **2022,** *5* (1), 1225.
15. Tan, Y.; Flynn, W. F.; Sivajothi, S.; Luo, D.; Bozal, S. B.; Davé, M.; Luciano, A. A.; Robson, P.; Luciano, D. E.; Courtois, E. T., Single-cell analysis of endometriosis reveals a coordinated transcriptional programme driving immunotolerance and angiogenesis across eutopic and ectopic tissues. *Nature cell biology* **2022,** *24* (8), 1306-1318.
16. Prather, G. R.; MacLean, J. A., 2nd; Shi, M.; Boadu, D. K.; Paquet, M.; Hayashi, K., Niclosamide As a Potential Nonsteroidal Therapy for Endometriosis That Preserves Reproductive Function in an Experimental Mouse Model. *Biology of reproduction* **2016,** *95* (4), 76.

17. Chen, W.; Mook, R. A., Jr.; Premont, R. T.; Wang, J., Niclosamide: Beyond an antihelminthic drug. *Cellular signalling* **2018,** *41*, 89-96.
18. Jug, M.; Laffleur, F.; Millotti, G., Revisiting Niclosamide Formulation Approaches - a Pathway Toward Drug Repositioning. *Drug design, development and therapy* **2024,** *18*, 4153-4182.
19. Rani, A.; Bisen, S.; Sharma, R.; Dar, A. I.; Sharma, A.; Dhull, A.; Palmer, N.; Goody, K. J.; Singh, N. K.; Sharma, A., Systemic targeting of aberrant neovascular tufts using trehalose-dendrimer nanocarriers for the treatment of proliferative retinopathies. *Theranostics* **2026,** *16* (3), 1504-1527.
20. Pulukuri, A. J.; Dhull, A.; Dar, A. I.; Rani, A.; Sharma, R.; Berkman, C. E.; Sharma, A., Dendrimer-Mediated Delivery Enhances Therapeutic Efficacy in Triple-Negative Breast Cancer. *Biomacromolecules* **2025,** *26* (9), 5979-6000.
21. Sharma, R.; Porterfield, J. E.; An, H.-T.; Jimenez, A. S.; Lee, S.; Kannan, S.; Sharma, A.; Kannan, R. M., Rationally Designed Galactose Dendrimer for Hepatocyte-Specific Targeting and Intracellular Drug Delivery for the Treatment of Liver Disorders. *Biomacromolecules* **2021,** *22* (8), 3574-3589.
22. Monge, P.; Søgaard, A. B.; Andersen, D. G.; Chandrawati, R.; Zelikin, A. N., Synthetic chemical ligands and cognate antibodies for biorthogonal drug targeting and cell engineering. *Advanced Drug Delivery Reviews* **2021,** *170*, 281-293.
23. Nam, H. Y.; Nam, K.; Hahn, H. J.; Kim, B. H.; Lim, H. J.; Kim, H. J.; Choi, J. S.; Park, J.-S., Biodegradable PAMAM ester for enhanced transfection efficiency with low cytotoxicity. *Biomaterials* **2009,** *30* (4), 665-673.
24. Huang, W.-C.; Lu, I. L.; Chiang, W.-H.; Lin, Y.-W.; Tsai, Y.-C.; Chen, H.-H.; Chang, C.-W.; Chiang, C.-S.; Chiu, H.-C., Tumortropic adipose-derived stem cells carrying smart nanotherapeutics for targeted delivery and dual-modality therapy of orthotopic glioblastoma. *Journal of Controlled Release* **2017,** *254*, 119-130.
25. Dhull, A.; Yu, C.; Wilmoth, A. H.; Chen, M.; Sharma, A.; Yiu, S., Dendrimers in Corneal Drug Delivery: Recent Developments and Translational Opportunities. *Pharmaceutics* **2023,** *15* (6).
26. Dhull, A.; Wei, J.; Pulukuri, A. J.; Rani, A.; Sharma, R.; Mesbahi, N.; Yoon, H.; Savoy, E. A.; Xaivong Vi, S.; Goody, K. J.; Berkman, C. E.; Wu, B. J.; Sharma, A., PSMA-targeted dendrimer as an efficient anticancer drug delivery vehicle for prostate cancer. *Nanoscale* **2024,** *16* (11), 5634-5652.
27. Dhull, A.; Zhang, Z.; Sharma, R.; Dar, A. I.; Rani, A.; Wei, J.; Gopalakrishnan, S.; Ghannam, A.; Hahn, V.; Pulukuri, A. J.; Tasevski, S.; Moughni, S.; Wu, B. J.; Sharma, A., Discovery of 2-deoxy glucose surfaced mixed layer dendrimer: a smart neuron targeted systemic drug delivery system for brain diseases. *Theranostics* **2024,** *14* (8), 3221-3245.
28. Dhull, A.; Park, K. W.; Dar, A. I.; Wang, A.; Rani, A.; Sharma, R.; Valdez, T. A.; Sharma, A., Mixed-Layered Glycodendrimer Probe for Imaging Inflammation at Surgical Site Infections. *ACS Sensors* **2025,** *10* (3), 2234-2243.
29. Puligujja, P.; McMillan, J.; Kendrick, L.; Li, T.; Balkundi, S.; Smith, N.; Veerubhotla, R. S.; Edagwa, B. J.; Kabanov, A. V.; Bronich, T.; Gendelman, H. E.; Liu, X. M., Macrophage folate receptor-targeted antiretroviral therapy facilitates drug entry, retention, antiretroviral activities and biodistribution for reduction of human immunodeficiency virus infections. *Nanomedicine : nanotechnology, biology, and medicine* **2013,** *9* (8), 1263-73.

30. Chandrupatla, D.; Molthoff, C. F. M.; Lammertsma, A. A.; van der Laken, C. J.; Jansen, G., The folate receptor β as a macrophage-mediated imaging and therapeutic target in rheumatoid arthritis. *Drug delivery and translational research* **2019,** *9* (1), 366-378.
31. Zheng, G. X.; Terry, J. M.; Belgrader, P.; Ryvkin, P.; Bent, Z. W.; Wilson, R.; Ziraldo, S. B.; Wheeler, T. D.; McDermott, G. P.; Zhu, J.; Gregory, M. T.; Shuga, J.; Montesclaros, L.; Underwood, J. G.; Masquelier, D. A.; Nishimura, S. Y.; Schnall-Levin, M.; Wyatt, P. W.; Hindson, C. M.; Bharadwaj, R.; Wong, A.; Ness, K. D.; Beppu, L. W.; Deeg, H. J.; McFarland, C.; Loeb, K. R.; Valente, W. J.; Ericson, N. G.; Stevens, E. A.; Radich, J. P.; Mikkelsen, T. S.; Hindson, B. J.; Bielas, J. H., Massively parallel digital transcriptional profiling of single cells. *Nature communications* **2017,** *8*, 14049.
32. Wang, W.; Vilella, F.; Alama, P.; Moreno, I.; Mignardi, M.; Isakova, A.; Pan, W.; Simon, C.; Quake, S. R., Single-cell transcriptomic atlas of the human endometrium during the menstrual cycle. *Nature medicine* **2020,** *26* (10), 1644-1653.
33. Lai, Z. Z.; Wang, Y.; Zhou, W. J.; Liang, Z.; Shi, J. W.; Yang, H. L.; Xie, F.; Chen, W. D.; Zhu, R.; Zhang, C.; Mei, J.; Zhao, J. Y.; Ye, J. F.; Zhang, T.; Li, M. Q., Single-cell transcriptome profiling of the human endometrium of patients with recurrent implantation failure. *Theranostics* **2022,** *12* (15), 6527-6547.
34. Garcia-Alonso, L.; Handfield, L. F.; Roberts, K.; Nikolakopoulou, K.; Fernando, R. C.; Gardner, L.; Woodhams, B.; Arutyunyan, A.; Polanski, K.; Hoo, R.; Sancho-Serra, C.; Li, T.; Kwakwa, K.; Tuck, E.; Lorenzi, V.; Massalha, H.; Prete, M.; Kleshchevnikov, V.; Tarkowska, A.; Porter, T.; Mazzeo, C. I.; van Dongen, S.; Dabrowska, M.; Vaskivskyi, V.; Mahbubani, K. T.; Park, J. E.; Jimenez-Linan, M.; Campos, L.; Kiselev, V. Y.; Lindskog, C.; Ayuk, P.; Prigmore, E.; Stratton, M. R.; Saeb-Parsy, K.; Moffett, A.; Moore, L.; Bayraktar, O. A.; Teichmann, S. A.; Turco, M. Y.; Vento-Tormo, R., Mapping the temporal and spatial dynamics of the human endometrium in vivo and in vitro. *Nature genetics* **2021,** *53* (12), 1698-1711.
35. Fonseca, M. A. S.; Haro, M.; Wright, K. N.; Lin, X.; Abbasi, F.; Sun, J.; Hernandez, L.; Orr, N. L.; Hong, J.; Choi-Kuaea, Y.; Maluf, H. M.; Balzer, B. L.; Fishburn, A.; Hickey, R.; Cass, I.; Goodridge, H. S.; Truong, M.; Wang, Y.; Pisarska, M. D.; Dinh, H. Q.; El-Naggar, A.; Huntsman, D. G.; Anglesio, M. S.; Goodman, M. T.; Medeiros, F.; Siedhoff, M.; Lawrenson, K., Single-cell transcriptomic analysis of endometriosis. *Nature genetics* **2023,** *55* (2), 255-267.
36. Huang, X.; Wu, L.; Pei, T.; Liu, D.; Liu, C.; Luo, B.; Xiao, L.; Li, Y.; Wang, R.; Ouyang, Y.; Zhu, H.; Huang, W., Single-cell transcriptome analysis reveals endometrial immune microenvironment in minimal/mild endometriosis. *Clinical and experimental immunology* **2023,** *212* (3), 285-295.
37. Marečková, M.; Garcia-Alonso, L.; Moullet, M.; Lorenzi, V.; Petryszak, R.; Sancho-Serra, C.; Oszlanczi, A.; Icoresi Mazzeo, C.; Wong, F. C. K.; Kelava, I.; Hoffman, S.; Krassowski, M.; Garbutt, K.; Gaitskell, K.; Yancheva, S.; Woon, E. V.; Male, V.; Granne, I.; Hellner, K.; Mahbubani, K. T.; Saeb-Parsy, K.; Lotfollahi, M.; Prigmore, E.; Southcombe, J.; Dragovic, R. A.; Becker, C. M.; Zondervan, K. T.; Vento-Tormo, R., An integrated single-cell reference atlas of the human endometrium. *Nature genetics* **2024,** *56* (9), 1925-1937.
38. Shin, S.; Chung, Y. J.; Moon, S. W.; Choi, E. J.; Kim, M. R.; Chung, Y. J.; Lee, S. H., Single-cell profiling identifies distinct hormonal, immunologic, and inflammatory signatures of endometriosis-constituting cells. *The Journal of pathology* **2023,** *261* (3), 323-334.
39. Han, J.; Gallerand, A.; Erlich, E. C.; Helmink, B. A.; Mair, I.; Li, X.; Eckhouse, S. R.; Dimou, F. M.; Shakhsheer, B. A.; Phelps, H. M.; Chan, M. M.; Mintz, R. L.; Lee, D. D.; Schilling, J. D.; Finlay, C. M.; Allen, J. E.; Jakubzick, C. V.; Else, K. J.; Onufer, E. J.; Zhang, N.; Randolph,

767 G. J., Human serous cavity macrophages and dendritic cells possess counterparts in the mouse
768 with a distinct distribution between species. *Nature immunology* **2024,** *25* (1), 155-165.
769 40. Zou, G.; Wang, J.; Xu, X.; Xu, P.; Zhu, L.; Yu, Q.; Peng, Y.; Guo, X.; Li, T.; Zhang, X.,
770 Cell subtypes and immune dysfunction in peritoneal fluid of endometriosis revealed by single-cell
771 RNA-sequencing. *Cell & bioscience* **2021,** *11* (1), 98.
772 41. Wolf, F. A.; Angerer, P.; Theis, F. J., SCANPY: large-scale single-cell gene expression data
773 analysis. *Genome biology* **2018,** *19* (1), 15.
774 42. Wolock, S. L.; Lopez, R.; Klein, A. M., Scrublet: Computational Identification of Cell
775 Doublets in Single-Cell Transcriptomic Data. *Cell systems* **2019,** *8* (4), 281-291.e9.
776 43. Giotti, B.; Chen, S. H.; Barnett, M. W.; Regan, T.; Ly, T.; Wiemann, S.; Hume, D. A.;
777 Freeman, T. C., Assembly of a parts list of the human mitotic cell cycle machinery. *Journal of*
778 *molecular cell biology* **2019,** *11* (8), 703-718.
779 44. Korsunsky, I.; Millard, N.; Fan, J.; Slowikowski, K.; Zhang, F.; Wei, K.; Baglaenko, Y.;
780 Brenner, M.; Loh, P. R.; Raychaudhuri, S., Fast, sensitive and accurate integration of single-cell
781 data with Harmony. *Nature methods* **2019,** *16* (12), 1289-1296.
782 45. Traag, V. A.; Waltman, L.; van Eck, N. J., From Louvain to Leiden: guaranteeing well-
783 connected communities. *Scientific reports* **2019,** *9* (1), 5233.
784 46. Soneson, C.; Robinson, M. D., Bias, robustness and scalability in single-cell differential
785 expression analysis. *Nature methods* **2018,** *15* (4), 255-261.
786 47. Wu, C.; Boey, D.; Bril, O.; Grootens, J.; Vijayabaskar, M. S.; Sorini, C.; Ekoff, M.; Wilson,
787 N. K.; Ungerstedt, J. S.; Nilsson, G.; Dahlin, J. S., Single-cell transcriptomics reveals the identity
788 and regulators of human mast cell progenitors. *Blood advances* **2022,** *6* (15), 4439-4449.
789 48. Panjwani, M. K.; Grassmann, S.; Sottile, R.; Le Luduec, J. B.; Kontopoulos, T.; van der
790 Ploeg, K.; Sun, J. C.; Hsu, K. C., Single-cell profiling aligns CD56(bright) and cytomegalovirus-
791 induced adaptive natural killer cells to a naïve-memory relationship. *Frontiers in immunology*
792 **2024,** *15*, 1499492.
793 49. Yu, G.; Wang, L. G.; Han, Y.; He, Q. Y., clusterProfiler: an R package for comparing
794 biological themes among gene clusters. *Omics : a journal of integrative biology* **2012,** *16* (5), 284-
795 7.
796 50. Nothnick, W. B.; Colvin, A.; Cheng, K. F.; Al-Abed, Y., Inhibition of macrophage
797 migration inhibitory factor reduces endometriotic implant size in mice with experimentally
798 induced disease. *Journal of endometriosis* **2011,** *3* (3), 135-142.
799 51. Herup-Wheeler, T.; Shi, M.; Harvey, M. E.; Talwar, C.; Kommagani, R.; MacLean, J. A.,
800 2nd; Hayashi, K., High-fat diets promote peritoneal inflammation and augment endometriosis-
801 associated abdominal hyperalgesia. *Frontiers in endocrinology* **2024,** *15*, 1336496.
802 52. Shi, M.; MacLean, J. A., 2nd; Hayashi, K., The involvement of peritoneal GATA6(+)
803 macrophages in the pathogenesis of endometriosis. *Frontiers in immunology* **2024,** *15*, 1396000.
804 53. Davies, L. C.; Rice, C. M.; Palmieri, E. M.; Taylor, P. R.; Kuhns, D. B.; McVicar, D. W.,
805 Peritoneal tissue-resident macrophages are metabolically poised to engage microbes using tissue-
806 niche fuels. *Nature communications* **2017,** *8* (1), 2074.
807 54. Vega-Pérez, A.; Villarrubia, L. H.; Godio, C.; Gutiérrez-González, A.; Feo-Lucas, L.;
808 Ferriz, M.; Martínez-Puente, N.; Alcaín, J.; Mora, A.; Sabio, G.; López-Bravo, M.; Ardavín, C.,
809 Resident macrophage-dependent immune cell scaffolds drive anti-bacterial defense in the
810 peritoneal cavity. *Immunity* **2021,** *54* (11), 2578-2594.e5.

55. Jiang, D.; Xiao, R.; Bai, J.; Wang, X.; Fang, Y.; Liu, J.; Wang, X.; Cui, M.; You, L.; Zhao, Y., FOLR2(+) macrophages in cancer: allies or enemies. *Cell communication and signaling : CCS* **2025,** *23* (1), 261.
56. Rani, A.; Pulukuri, A. J.; Wei, J.; Dhull, A.; Dar, A. I.; Sharma, R.; Mesbahi, N.; Savoy, E. A.; Yoon, H.; Wu, B. J.; Berkman, C. E.; Sharma, A., PSMA-Targeted 2-Deoxyglucose-Based Dendrimer Nanomedicine for the Treatment of Prostate Cancer. *Biomacromolecules* **2024,** *25* (9), 6164-6180.
57. Dar, A. I.; Jain, V.; Rani, A.; Pulukuri, A. J.; Gonzalez, J. C.; Dhull, A.; Sharma, R.; Sharma, A., Silibinin-Conjugated Galactose Dendrimers for Targeted Treatment of Hepatocellular Carcinoma. *ACS Applied Materials & Interfaces* **2025,** *17* (14), 20980-21000.
58. Dar, A. I.; Zhang, Z.; Gopalakrishnan, S.; Sharma, R.; Pulukuri, A. J.; Rani, A.; Dhull, A.; Gonzalez, J. C.; Atoui, T.; Mashal, Y.; Naseer, Z.; Calmi, J.; Sharma, A., Neuron-targeted 2-deoxyglucose-dendrimer-rosiglitazone nanotherapy mitigates neuroinflammation and cognitive deficits in pediatric traumatic brain injury. *Bioengineering & Translational Medicine n/a* (n/a), e70053.
59. Chen, C.; Ke, J.; Zhou, X. E.; Yi, W.; Brunzelle, J. S.; Li, J.; Yong, E. L.; Xu, H. E.; Melcher, K., Structural basis for molecular recognition of folic acid by folate receptors. *Nature* **2013,** *500* (7463), 486-9.
60. van Dongen, M. A.; Silpe, J. E.; Dougherty, C. A.; Kanduluru, A. K.; Choi, S. K.; Orr, B. G.; Low, P. S.; Banaszak Holl, M. M., Avidity mechanism of dendrimer-folic acid conjugates. *Molecular pharmaceutics* **2014,** *11* (5), 1696-706.
61. Hong, S.; Leroueil, P. R.; Majoros, I. J.; Orr, B. G.; Baker, J. R., Jr.; Banaszak Holl, M. M., The binding avidity of a nanoparticle-based multivalent targeted drug delivery platform. *Chemistry & biology* **2007,** *14* (1), 107-15.
62. Thomas, T. P.; Huang, B.; Choi, S. K.; Silpe, J. E.; Kotlyar, A.; Desai, A. M.; Zong, H.; Gam, J.; Joice, M.; Baker, J. R., Jr., Polyvalent dendrimer-methotrexate as a folate receptor-targeted cancer therapeutic. *Molecular pharmaceutics* **2012,** *9* (9), 2669-2676.
63. de Souza, H. M. R.; Guedes, J. S.; Freitas, R.; Gelves, L. G. V.; Fokoue, H. H.; Sant'Anna, C. M. R.; Barreiro, E. J.; Lima, L. M., Comparative chemical and biological hydrolytic stability of homologous esters and isosteres. *Journal of enzyme inhibition and medicinal chemistry* **2022,** *37* (1), 718-727.
64. Kim, J. H.; Park, S.; Jung, E.; Shin, J.; Kim, Y. J.; Kim, J. Y.; Sessler, J. L.; Seo, J. H.; Kim, J. S., A dual-action niclosamide-based prodrug that targets cancer stem cells and inhibits TNBC metastasis. *Proceedings of the National Academy of Sciences of the United States of America* **2023,** *120* (21), e2304081120.
65. Li, J.; Chang, Y.; Zou, Z. Z., Enhancing the in vivo bioavailability and absorption of Niclosamide with amorphous solid dispersion via solvent method. *RPS Pharmacy and Pharmacology Reports* **2024,** *3* (4).
66. Navath, R. S.; Kurtoglu, Y. E.; Wang, B.; Kannan, S.; Romero, R.; Kannan, R. M., Dendrimer-drug conjugates for tailored intracellular drug release based on glutathione levels. *Bioconjugate chemistry* **2008,** *19* (12), 2446-55.

854 **Figure legends**

855 **Figure 1. scRNA-seq analysis of FOLR2$^+$ macrophages in endometrium and pelvic exudate**
856 **cells in endometriosis.** (**A, B**) Lists of human scRNA-seq datasets analyzed and sample size per
857 dataset in the groups of (**A**) eutopic endometrium with (EuE) and without (Cont) endometriosis,
858 ectopic endometrium (lesion, EcE), and (**B**) pelvic exudate cells from subjects with (Endo) and
859 without (Cont) endometriosis. (**C, D**) UMAP plots showing major cell types identified in the
860 endometrium (EM) and pelvic cells (P). (**E, F**) Violin plot representing marker gene expression
861 for each major cell type identified in the endometrial and pelvic cell datasets. (**G, H**) UMAP
862 projections showing the expression patterns of FOLR2 in the endometrial and pelvic cells. (**I, J**)
863 Bar plots showing enriched gene ontology (GO) biological processes in the FOLR2$^+$ macrophages
864 from the endometrium and pelvic cells. (**K, L**) The proportions of endometrial and pelvic FOLR2-
865 expressing cells to total cells within each tissue type. Differences among groups were analyzed
866 with one-way ANOVA followed by Tukey's multiple comparisons. **P<0.01, ***P<0.001. (**M,**
867 **N**) Dot plot showing representative significantly differentially expressed genes (DEGs) involved
868 in the proinflammatory, angiogenesis, and adhesion processes among groups of endometrium and
869 pelvic cells (pvals_adj <0.05).

870

871 **Figure 2. Preparation and structural elucidation of FA-2DG-D-Cy5 conjugate.** (**A**) Schematic
872 representation for the synthesis of FA-2DG-D-Cy5 using CuAAC reaction. Reagents and
873 conditions: (i) DMSO, DCC, NHS, DIPEA, RT, 12 hours, 70% (ii) DMF, EDC.HCl, DMAP, RT,
874 12 hours, 80% (iii) $CuSO_4.5H_2O$, Sodium ascorbate, DMF, DI Water, 60 ºC, 10 hours, 84% (iv)
875 $CuSO_4.5H_2O$, Sodium ascorbate, DMF, DI Water, 40 ºC, 6 hours, 88% (**B**) ^{1}H NMR spectra
876 showing characteristic proton signals of 2DG-D, 2DG-D-Hexyne, Folic Acid, FA-Azide, FA-2DG-
877 D and FA-2DG-D-Cy5 at each step of the synthesis.

878

879 **Figure 3: In vivo and ex vivo fluorescence imaging and whole-body biodistribution of FA-**
880 **2DG-D-Cy5**. (**A**) Whole-body in vivo fluorescence images of mice following intravenous (tail
881 vein) administration of FA-2DG-D-Cy5 in sham controls (left) and ELL-induced mice (right), or
882 2DG-D-Cy5 administered to ELL-induced mice (center) at 1, 6, 24, and 72 hours (n =
883 3/group/timepoint). (**B**) Ex vivo fluorescence images of major organs collected at 72 hours post-
884 injection. Organs are arranged from top to bottom as: brain, heart, spleen, lungs, liver, kidneys,
885 and lesion. (**C**) Quantitative analysis of in vivo fluorescence signals in major organs at 72 hours
886 (n = 3). (**D**) Heat map showing the mean percentage of injected dose in lesions and major organs
887 at 1, 6, 24, and 72 hours after FA-2DG-D-Cy5 administration in sham controls and ELL-induced
888 mice, or ELL-induced mice treated with 2DG-D-Cy5 (n=3/group). Heatmap was generated with
889 the ComplexHeatmap package of R. (**E**) Quantitative biodistribution of FA-2DG-D-Cy5 and 2DG-
890 D-Cy5 in lesions and major organs at 72 hours in sham and ELL-induced mice (n = 3). Data for
891 (D) and (E) were obtained by fluorescence spectroscopy of homogenized tissues and are shown as
892 the percentage of the injected dose per organ. Differences in each tissue among groups for data in
893 (C) and (E) were analyzed by one-way ANOVA followed by Tukey's multiple-comparison test. p
894 < 0.05 (*), $p < 0.01$ (**). ELL, endometriosis-like lesion.

895

896 **Figure 4: Cellular uptake of FA-2DG-D-Cy5 and 2DG-D-Cy5 at 2 weeks following**
897 **intraperitoneal administration.** Representative images showing selective uptake of FA-2DG-D-
898 Cy5 or 2DG-D-Cy5 **(A)** in the peritoneum, **(B)** in endometriosis-like lesions (ELL), and **(C)**
899 kidney, liver, and spleen from ELL-induced mice (n=3). Peritoneal cells and tissues were co-
900 stained with FRβ (green) and DAPI (blue). The Cy5 signal (red) was directly acquired with a
901 Confocal Microscope. White arrows show Cy5-positive signal in $FR\beta^+$ cells.

902

903 **Figure 5. Preparation and structural elucidation of FA-2DG-D-Niclo conjugate.** (**A**)
904 Schematic representation for the synthesis of **(i)** Niclo-Azide and **(ii)** FA-2DG-D-Niclo using
905 CuAAC reaction. Reagents and conditions: (i) DCM, HCl, Dioxane, RT, 3 hours (ii) DCM, TEA,
906 Triphosgene, -25 ºC, 1 hour (iii) DCM, TEA, DMAP, RT, 16 hours, 49% (iv) DMF, EDC.HCl,
907 DMAP, RT, 12 hours, 82% (v) $CuSO_4.5H_2O$, Sodium ascorbate, DMF, DI Water, 60 ºC, 10 hours,
908 85% (vi) $CuSO_4.5H_2O$, Sodium ascorbate, DMF, DI Water, 40 ºC, 10 hours, 75% (**B**) ^1H NMR

909 spectra showing characteristic proton signals of FA-2DG-D', Compound 10, Niclosamide, Niclo-
910 Azide and FA-2DG-D-Niclo at each step of the synthesis.

911

912 **Figure 6**. **Characterization of FA-2DG-D-Niclo conjugate and intermediates:** (**A**) HPLC
913 chromatograms of intermediates at various synthesis steps and percentage purity of FA-2DG-D-
914 Niclo. (**B**) (i) Hydrodynamic diameter, and (ii) Zeta Potential of FA-2DG-D analyzed by dynamic
915 light scattering (DLS) in triplicates. (**C**) (i) Hydrodynamic diameter, and (ii) Zeta Potential of FA-
916 2DG-D-Niclo analyzed by dynamic light scattering (DLS) in triplicates.

917

918 **Figure 7**. **Characterization of FA-2DG-D-Niclo conjugate and intermediates:** (**A**) Table
919 showing the physicochemical properties of FA-2DG-D-Niclo and image showing the increase in
920 solubility of niclosamide after conjugation with FA-2DG-D scaffold (FA-2DG-D-Niclo). (**B**) The
921 figure shows the reproducibility in the synthesis of multiple 400 mg-scale batches of FA-2DG-D-
922 Niclo via ^{1}H NMR and HPLC. The ^{1}H NMR spectra of 3 batches (400 mg scale) show
923 characteristic protons from FA-2DG-D-Niclo. The HPLC chromatographs show reproducibility in
924 the purity of these batches with all these batches showing >99% purity. (**C**) In vitro drug release
925 profile of FA-2DG-D-Niclo conjugate in PBS and 0.1mM GSH, intracellular conditions at 37ºC
926 after 15 days, and in (100%) human plasma after 120 hours.

927

928 **Figure 8**. **Quantitative analysis of FRβ^{+} cells in the lesion and peritoneum following**
929 **dendrimer treatments.** (**A**) Study design as described in the Methods. (**B**) Representative
930 immunohistochemical images (left) and quantification of FRβ^{+} cells (right) in the lesions at Day
931 14 and Day 21 after lesion induction (n=3-8, as dendrimer-Niclo inhibited lesion development). A
932 one-way ANOVA followed by Tukey's multiple-comparison test was used to assess differences
933 among groups. **(C)** Representative flow plots (left) and quantification of peritoneal FRβ^{+} cells
934 (right). Differences in peritoneal FRβ^{+} cells among groups at each time point were assessed by the
935 Kruskal-Wallis test. Data in all figures are shown as the mean ± SEM (n=8). $p < 0.05$ (*), or $p <$
936 0.01 (**).

937

938 **Figure 9**. **Efficacy of FA-2DG-D-Niclo on treating endometriosis.** (**A**) Quantification of lesion
939 numbers and volumes in mice at Days 14 and 21 after the lesion induction. Lesion volumes were
940 calculated by length × width^2. Differences in lesion number and volume among groups at each
941 time point were assessed by the Kruskal-Wallis test. (**B**) Evaluation of endometriosis-associated
942 hyperalgesia. Abdominal (left) and hindpaw (right) withdrawal thresholds were assessed by the
943 von Frey test. The data represent the group mean threshold at the corresponding time point (n=16
944 at Day -1 and Day 7, n=8 at Day 14 and Day 21). Red arrows show the time of i.p.
945 administration of FA-2DG-D or FA-2DG-D-Niclo. The time-course differences within each
946 treatment group were compared with a Kruskal-Wallis test followed by Dunnett's multiple-
947 comparison test. The colored stars or ns (non-significance) represent the differences at the
948 corresponding time point to Day -1 within the treatment group. To compare the dosing effects of
949 niclosamide at each time point among groups, the Kruskal-Wallis test was used. Data are shown
950 as the *mean ± SEM (n=8). $p < 0.05$ (*), $p < 0.01$ (**), $p < 0.001$ (***), or $p < 0.0001$ (****).*

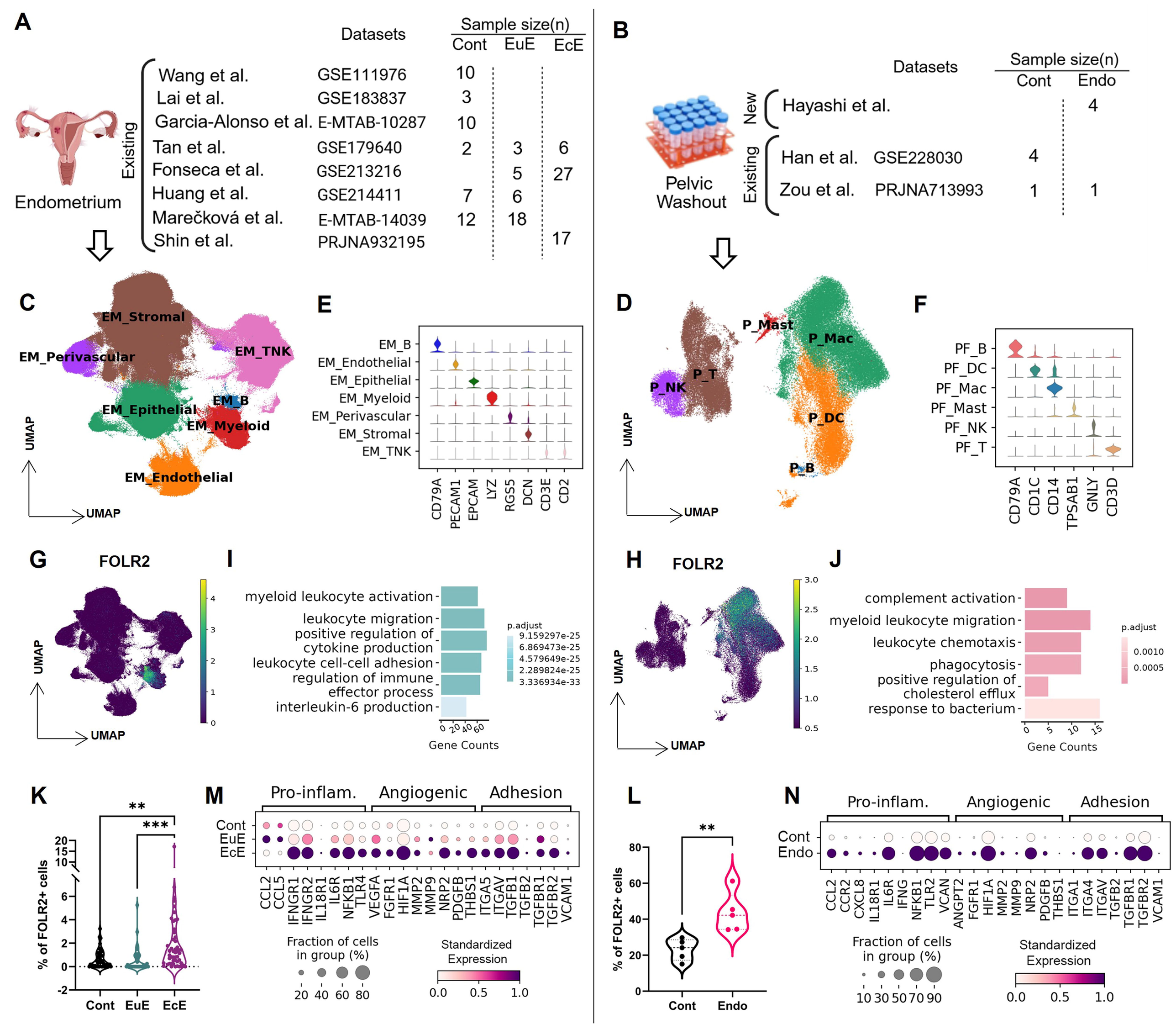
A
Datasets
Sample size(n)
Cont
EuE
EcE
Existing
Wang et al. GSE111976 10
Lai et al. GSE183837 3
Garcia-Alonso et al. E-MTAB-10287 10
Tan et al. GSE179640 2 3 6
Fonseca et al. GSE213216 5 27
Huang et al. GSE214411 7 6
Marečková et al. E-MTAB-14039 12 18
Shin et al. PRJNA932195 17
Endometrium
B
Datasets
Sample size(n)
Cont
Endo
New
Hayashi et al. 4
Existing
Han et al. GSE228030 4
Zou et al. PRJNA713993 1 1
Pelvic Washout
C
EM_Stromal
EM_Perivascular
EM_TNK
EM_Epithelial
EM_B
EM_Myeloid
EM_Endothelial
UMAP
UMAP
D
P_Mast
P_Mac
P_T
P_NK
P_DC
P_B
UMAP
UMAP
E
EM_B
EM_Endothelial
EM_Epithelial
EM_Myeloid
EM_Perivascular
EM_Stromal
EM_TNK
CD79A
PECAM1
EPCAM
LYZ
RGS5
DCN
CD3E
CD2
F
PF_B
PF_DC
PF_Mac
PF_Mast
PF_NK
PF_T
CD79A
CD1C
CD14
TPSAB1
GNLY
CD3D
G
FOLR2
UMAP
UMAP
H
FOLR2
UMAP
UMAP
I
myeloid leukocyte activation
leukocyte migration
positive regulation of cytokine production
leukocyte cell-cell adhesion
regulation of immune effector process
interleukin-6 production
p.adjust
9.159297e-25
6.869473e-25
4.579649e-25
2.289824e-25
3.336934e-33
Gene Counts
J
complement activation
myeloid leukocyte migration
leukocyte chemotaxis
phagocytosis
positive regulation of cholesterol efflux
response to bacterium
p.adjust
0.0010
0.0005
Gene Counts
K
% of FOLR2+ cells
Cont
EuE
EcE
L
% of FOLR2+ cells
Cont
Endo
M
Pro-inflam.
Angiogenic
Adhesion
Cont
EuE
EcE
CCL2
CCL5
IFNGR1
IFNGR2
IL18R1
IL6R
NFKB1
TLR4
VEGFA
FGFR1
HIF1A
MMP2
MMP9
NRP2
PDGFB
THBS1
ITGA5
ITGAV
TGFB1
TGFB2
TGFBR1
TGFBR2
VCAM1
Fraction of cells in group (%)
Standardized Expression
N
Pro-inflam.
Angiogenic
Adhesion
Cont
Endo
CCL2
CCR2
CXCL8
IL18R1
IL6R
IFNG
NFKB1
TLR2
VCAN
ANGPT2
FGFR1
HIF1A
MMP2
MMP9
NRP2
PDGFB
THBS1
ITGA1
ITGA4
ITGAV
TGFB2
TGFBR1
TGFBR2
VCAM1
Fraction of cells in group (%)
Standardized Expression

A. Synthesis of FA-2DG-D-Cy5

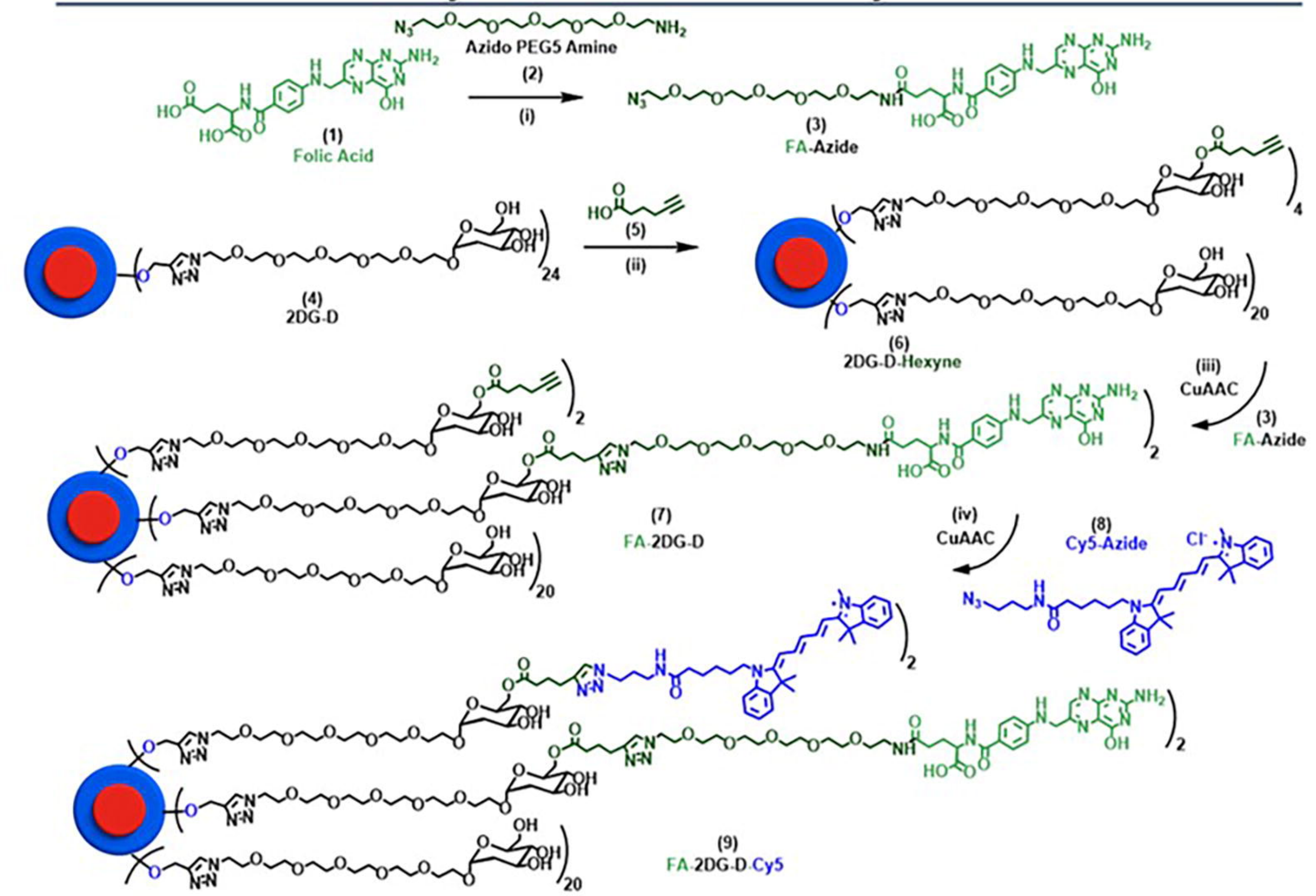

B. ^{1}H NMR Characterization of FA-2DG-D-Cy5

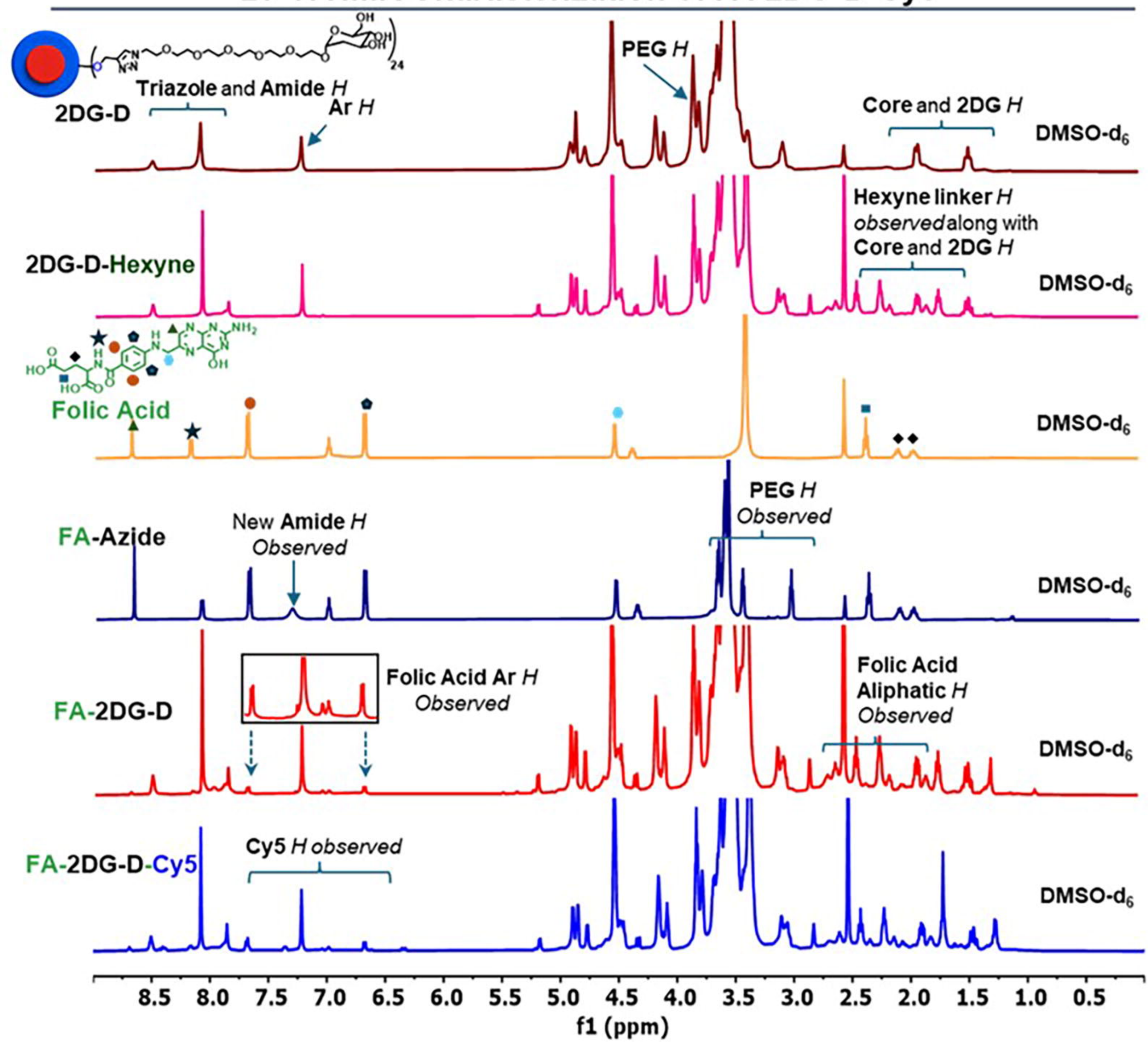

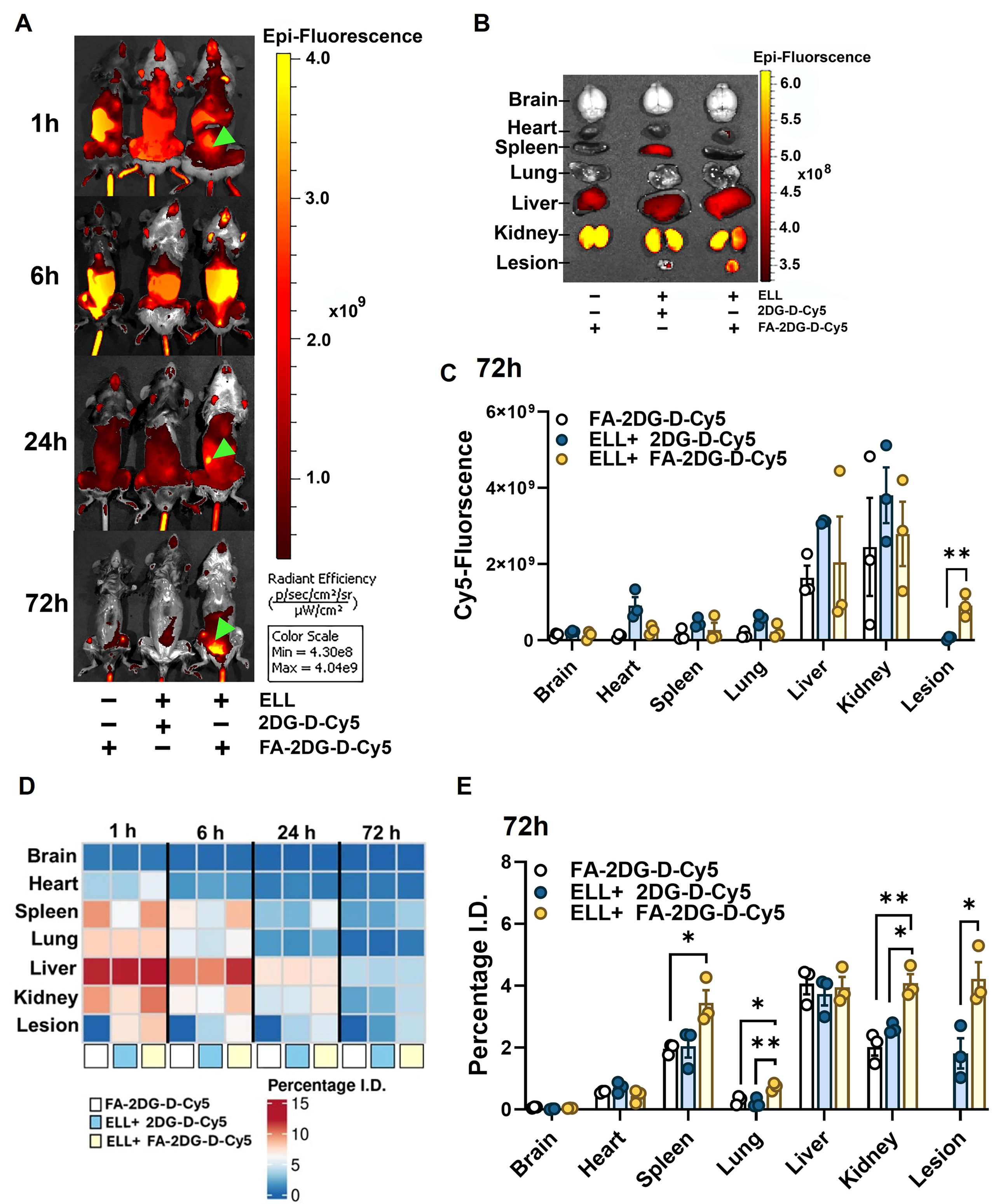
A
Epi-Fluorescence
4.0
3.0
2.0
1.0
x10^9
1h
6h
24h
72h
Radiant Efficiency
(p/sec/cm²/sr / µW/cm²)
Color Scale
Min = 4.30e8
Max = 4.04e9
− + + ELL
− + − 2DG-D-Cy5
+ − + FA-2DG-D-Cy5
B
Epi-Fluorscence
Brain
Heart
Spleen
Lung
Liver
Kidney
Lesion
6.0
5.5
5.0
x10^8
4.5
4.0
3.5
− + + ELL
− + − 2DG-D-Cy5
+ − + FA-2DG-D-Cy5
C 72h
Cy5-Fluorscence
6×10^9
4×10^9
2×10^9
0
FA-2DG-D-Cy5
ELL+ 2DG-D-Cy5
ELL+ FA-2DG-D-Cy5
**
Brain
Heart
Spleen
Lung
Liver
Kidney
Lesion
D
1 h
6 h
24 h
72 h
Brain
Heart
Spleen
Lung
Liver
Kidney
Lesion
FA-2DG-D-Cy5
ELL+ 2DG-D-Cy5
ELL+ FA-2DG-D-Cy5
Percentage I.D.
15
10
5
0
E
72h
Percentage I.D.
8
6
4
2
0
FA-2DG-D-Cy5
ELL+ 2DG-D-Cy5
ELL+ FA-2DG-D-Cy5
*
**
*
**
*
Brain
Heart
Spleen
Lung
Liver
Kidney
Lesion

A. Peritoneal cells

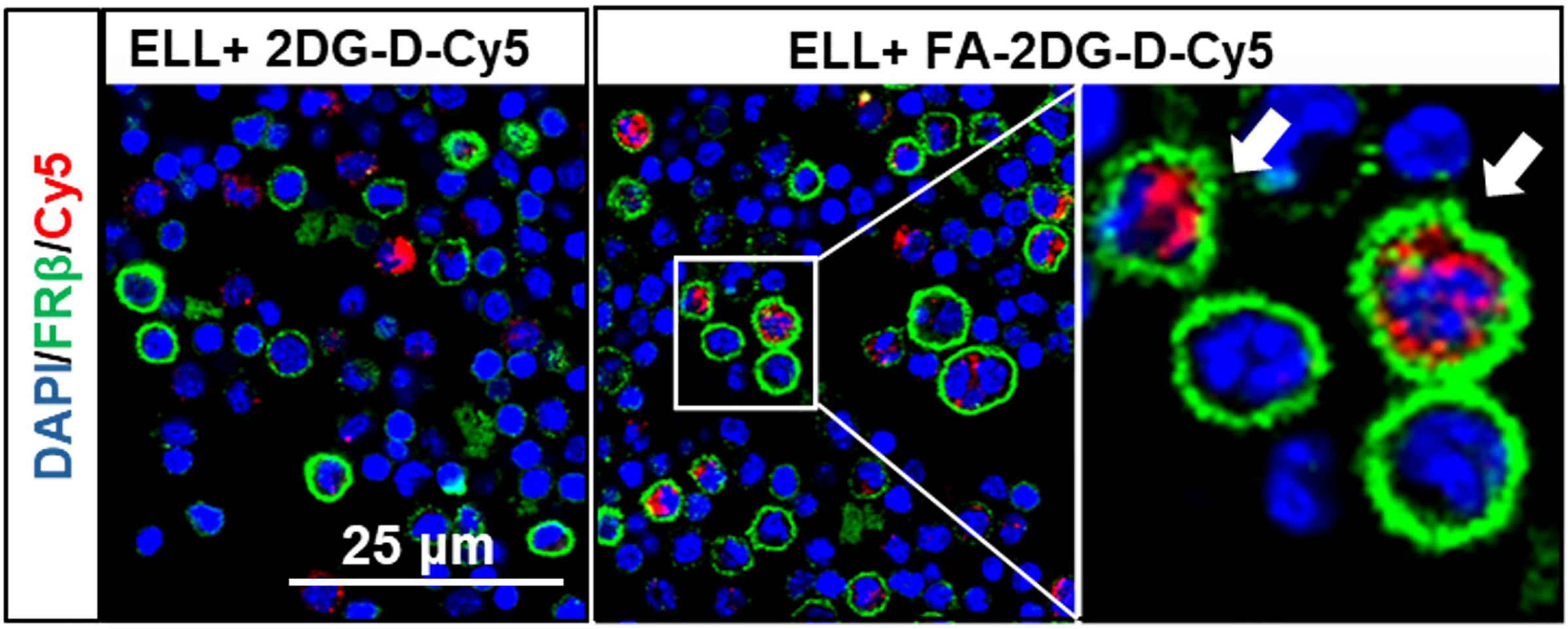

B. Lesions

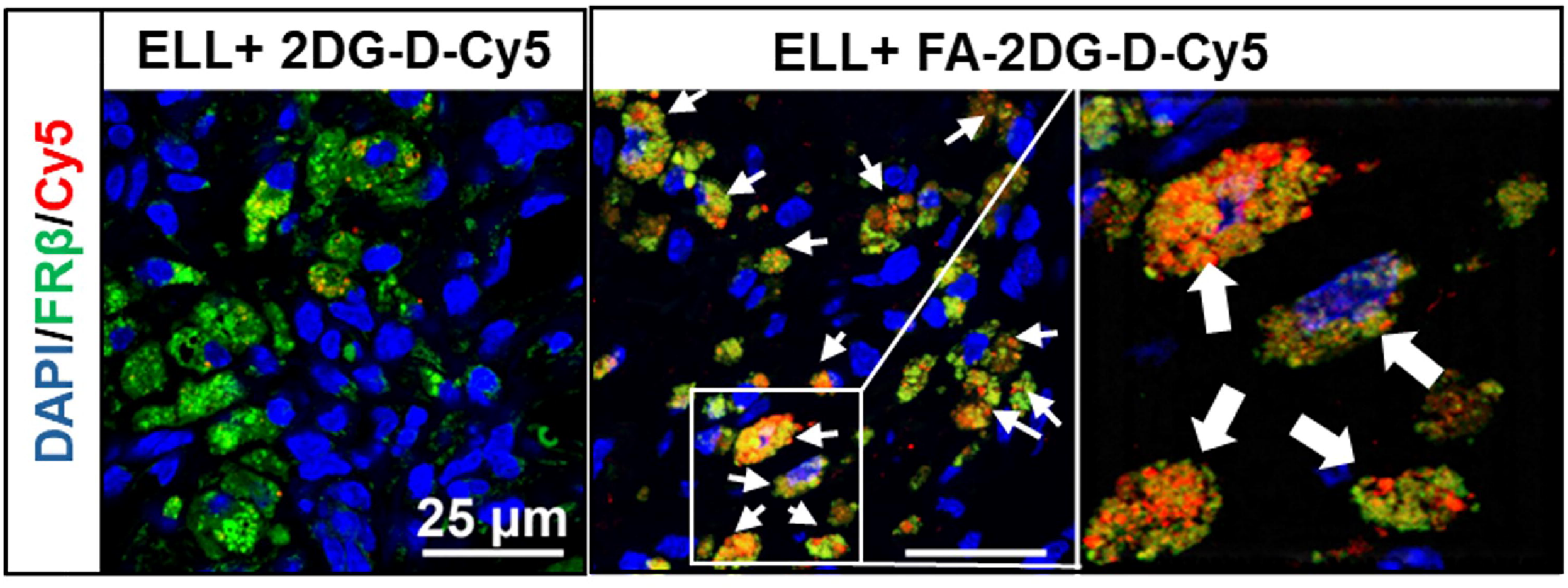

C. Major organs

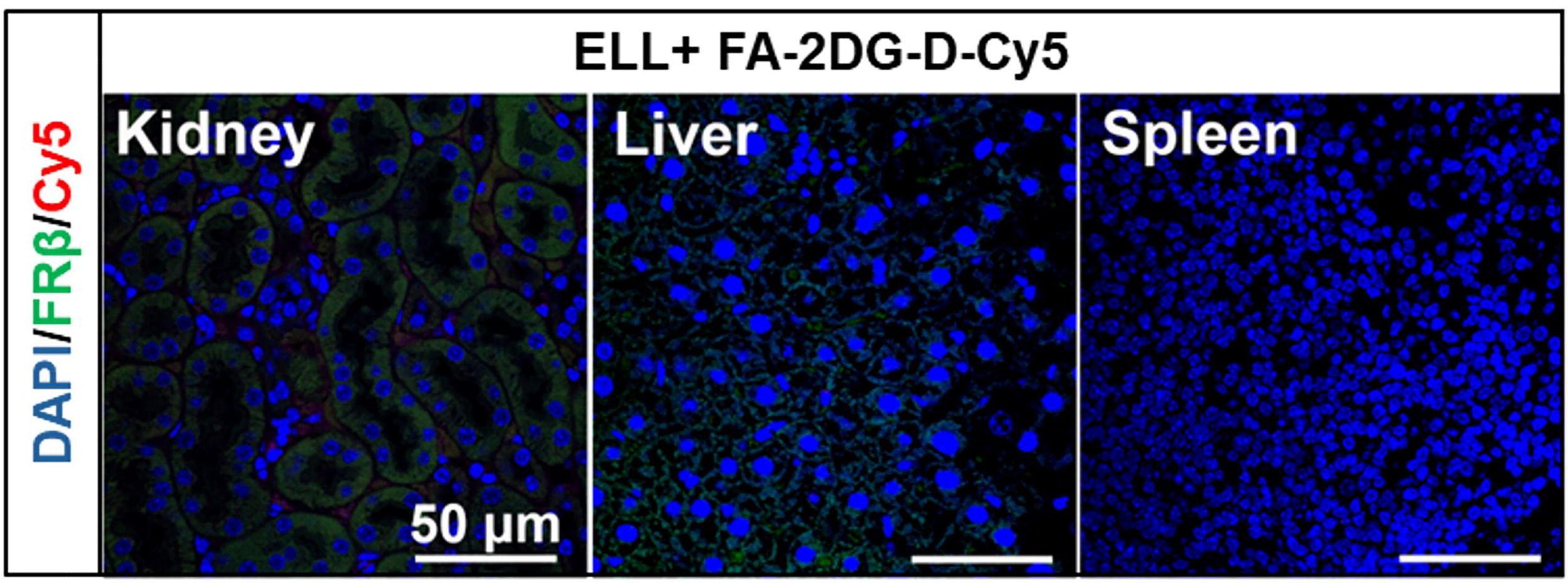

A. Synthesis of FA-2DG-D-Niclo

(i) Synthesis of Niclo-Azide

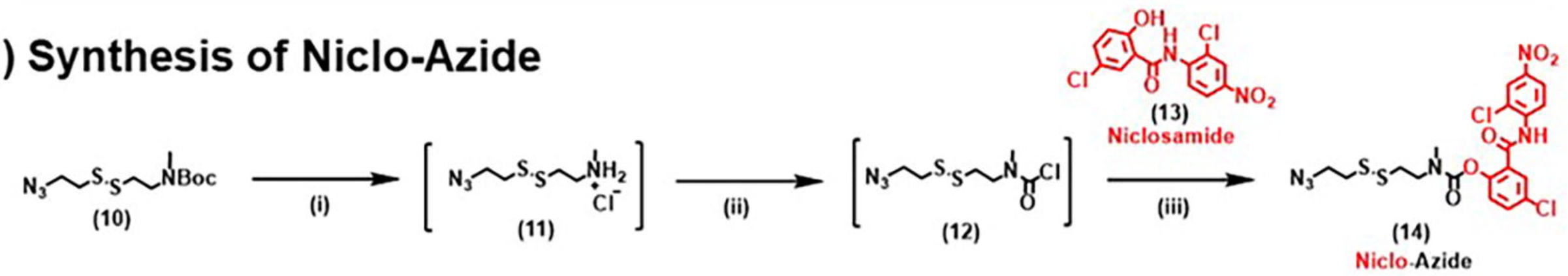

(ii) Synthesis of FA-2DG-D-Niclo

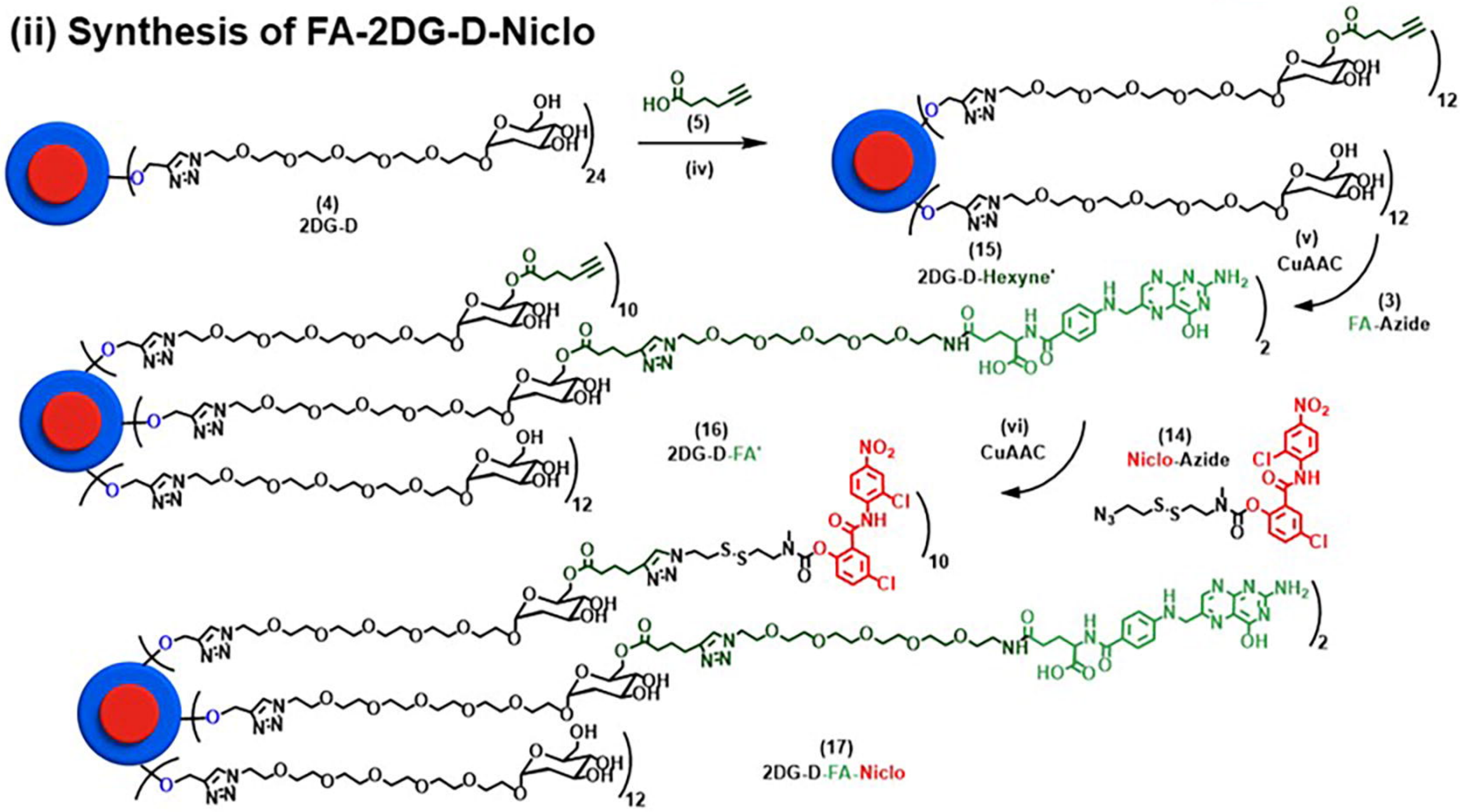

B. ^{1}H NMR Characterization of FA-2DG-D-Niclo

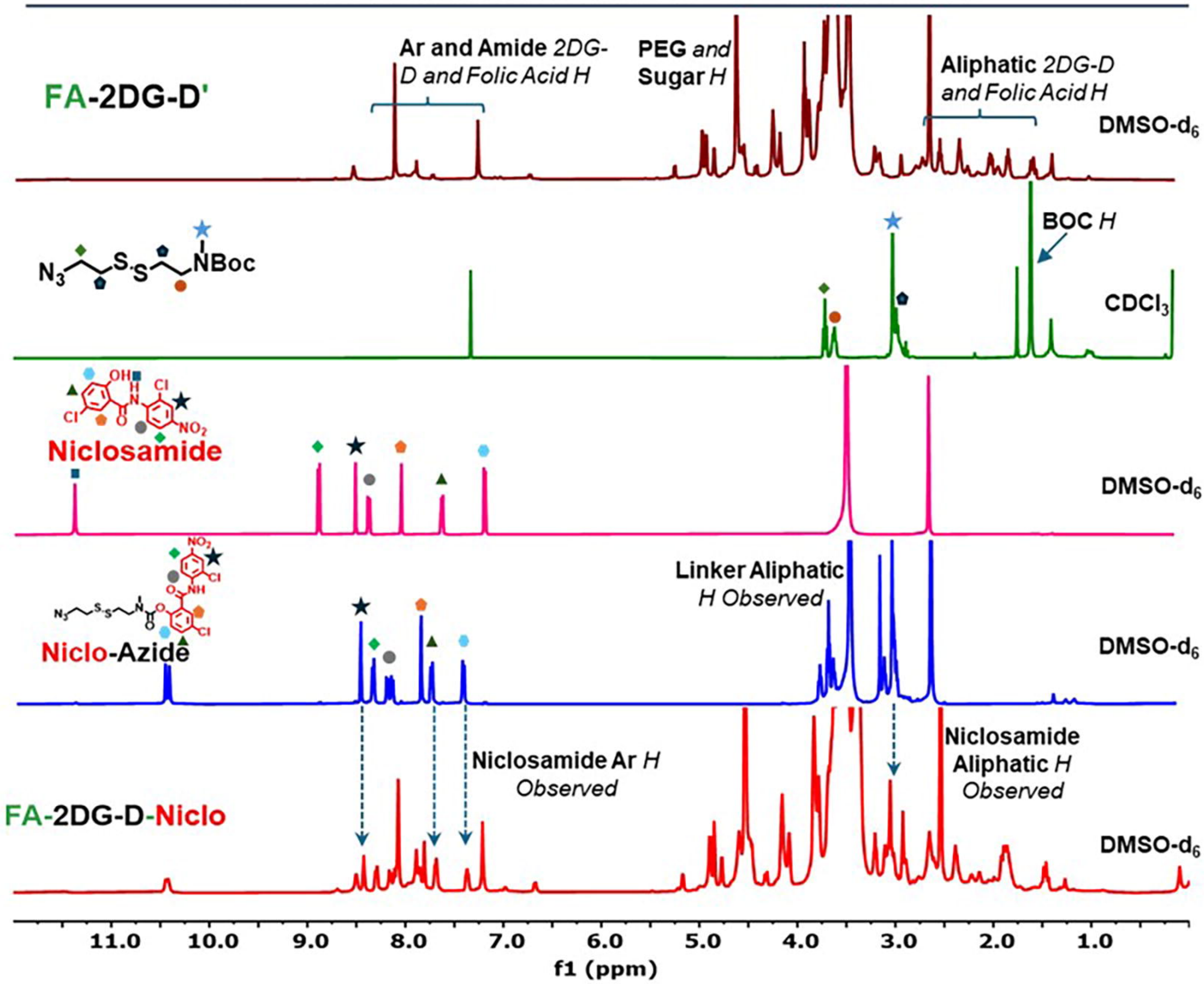

A. HPLC Characterization of FA-2DG-D-Niclo

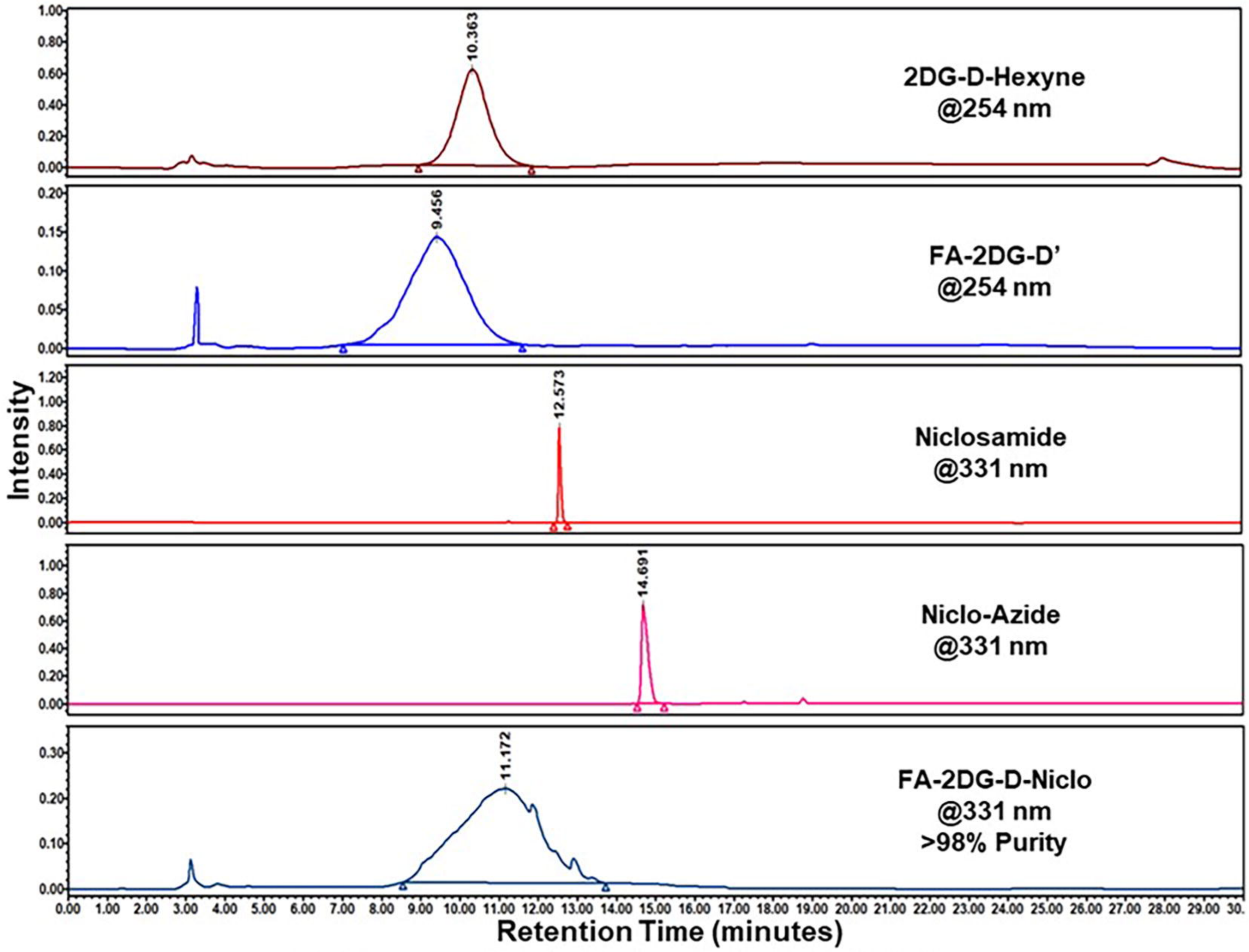

B. Size and Zeta Potential of FA-2DG-D

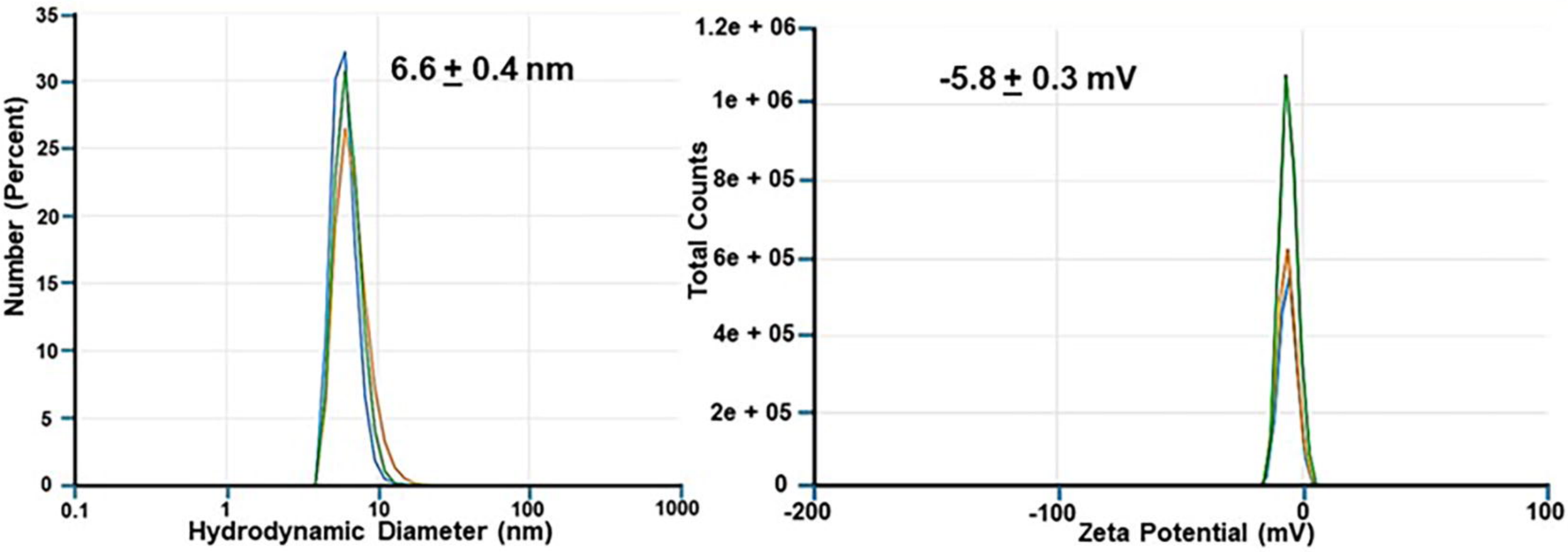

C. Size and Zeta Potential of FA-2DG-D-Niclo

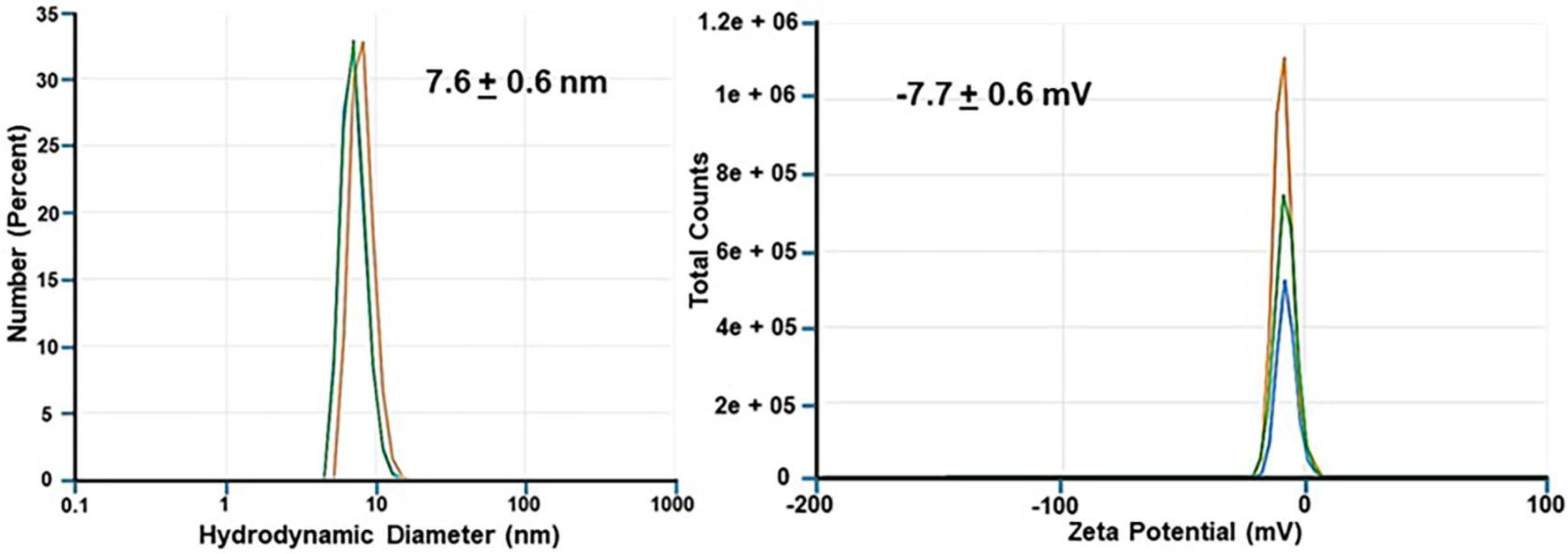

A. Reproducible Synthesis of FA-2DG-D-Niclo

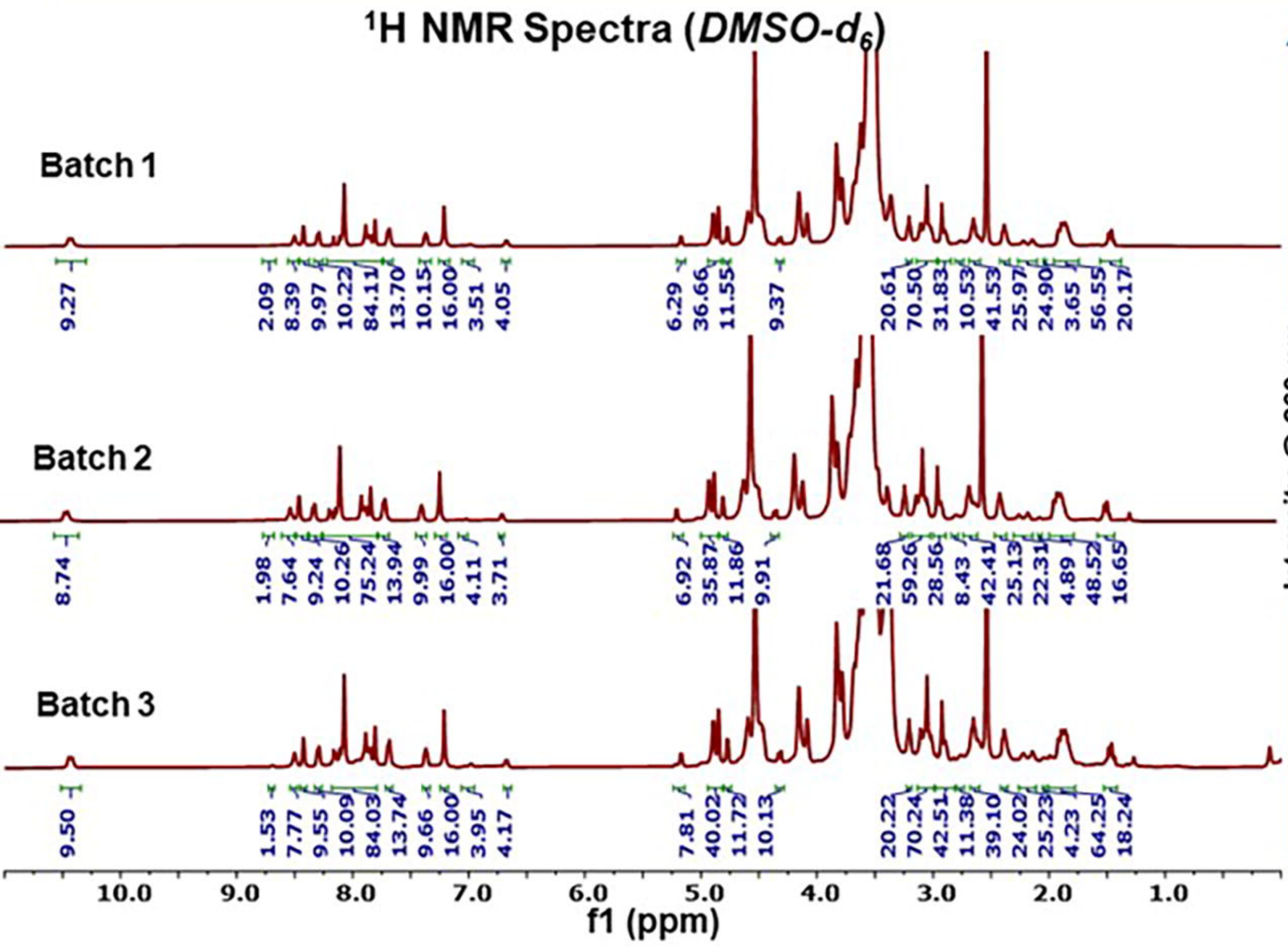

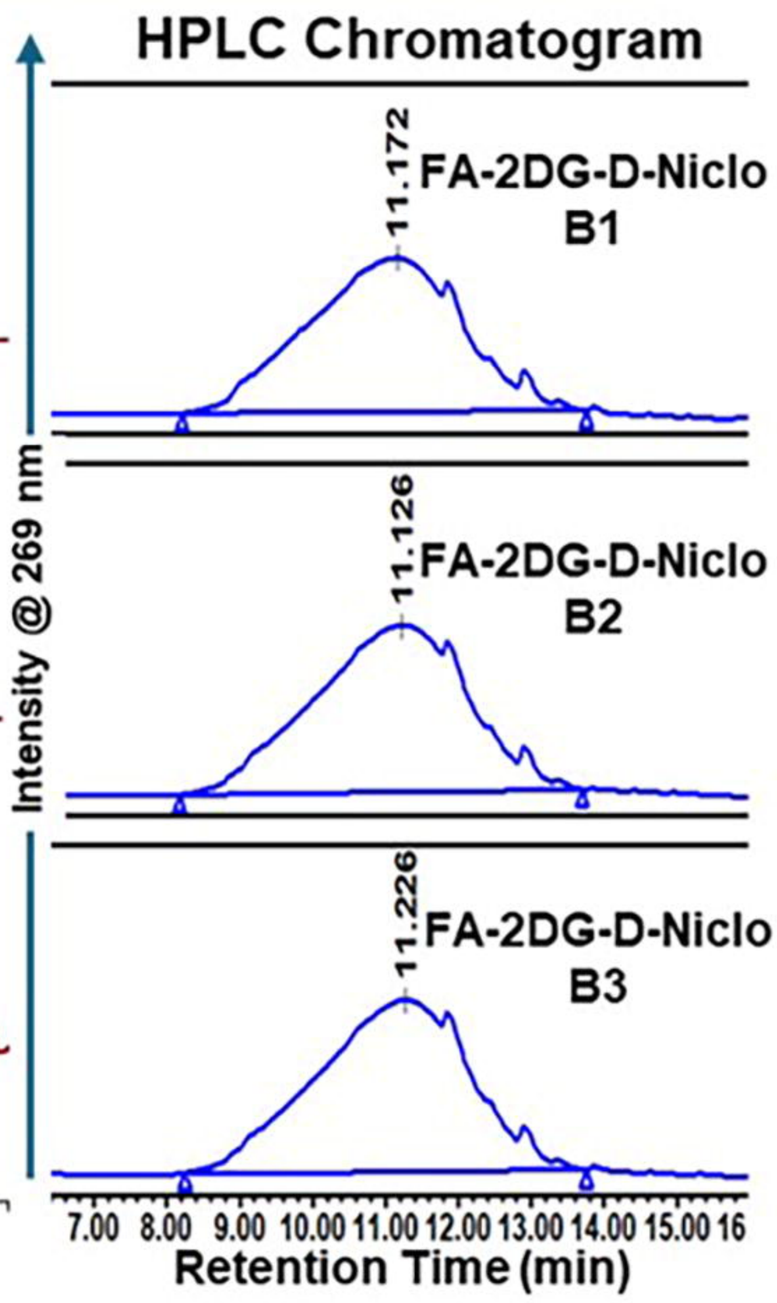

B. Physicochemical Properties and Solubility of FA-2DG-D-Niclo

Physicochemical Properties of FA-2DG-D-Niclo	
Hydrodynamic Diameter	7.6 ± 0.6 nm
Zeta Potential	-7.7 ± 0.6 mV
HPLC Purity	>98%
Drug Loading	~12%
Solubility	150 mg/mL

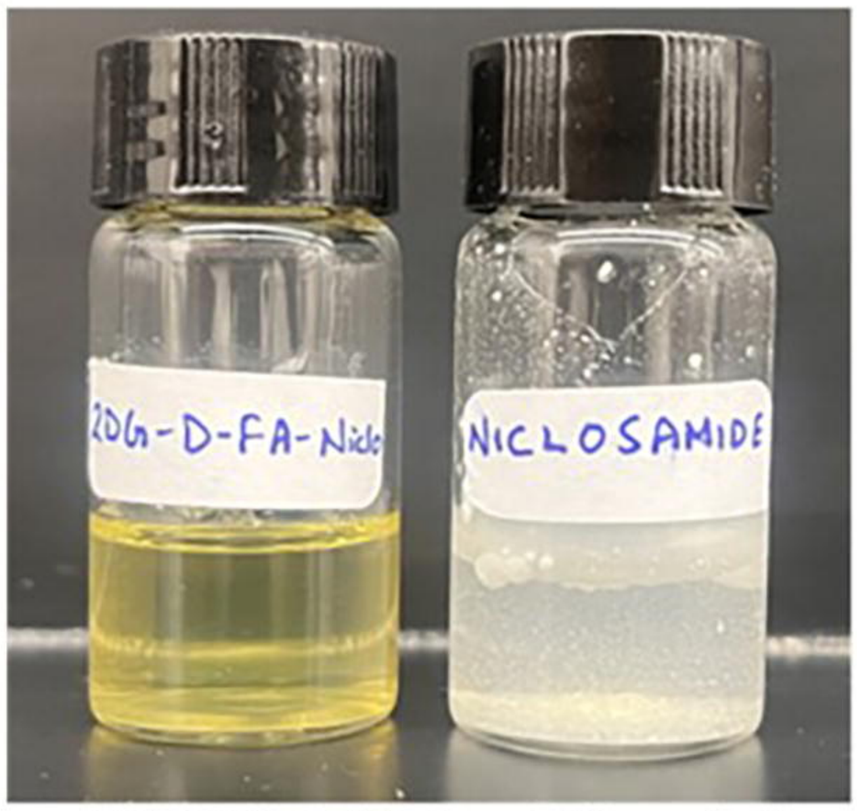

1. FA-2DG-D-Niclo at 18 mg/mL (Niclosamide equivalent concentration)
2. Niclosamide at 1 mg/mL

C. *In Vitro* Drug Release Profile of FA-2DG-D-Niclo

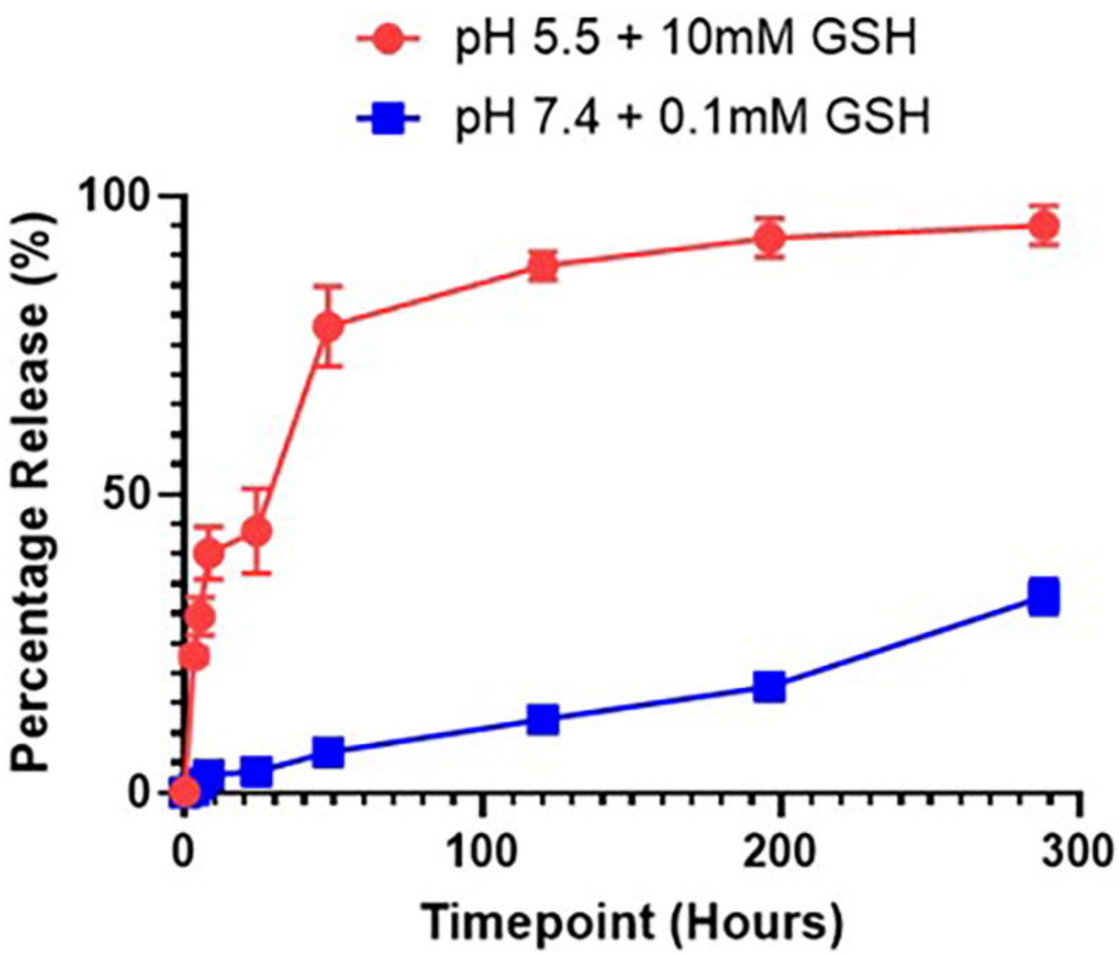

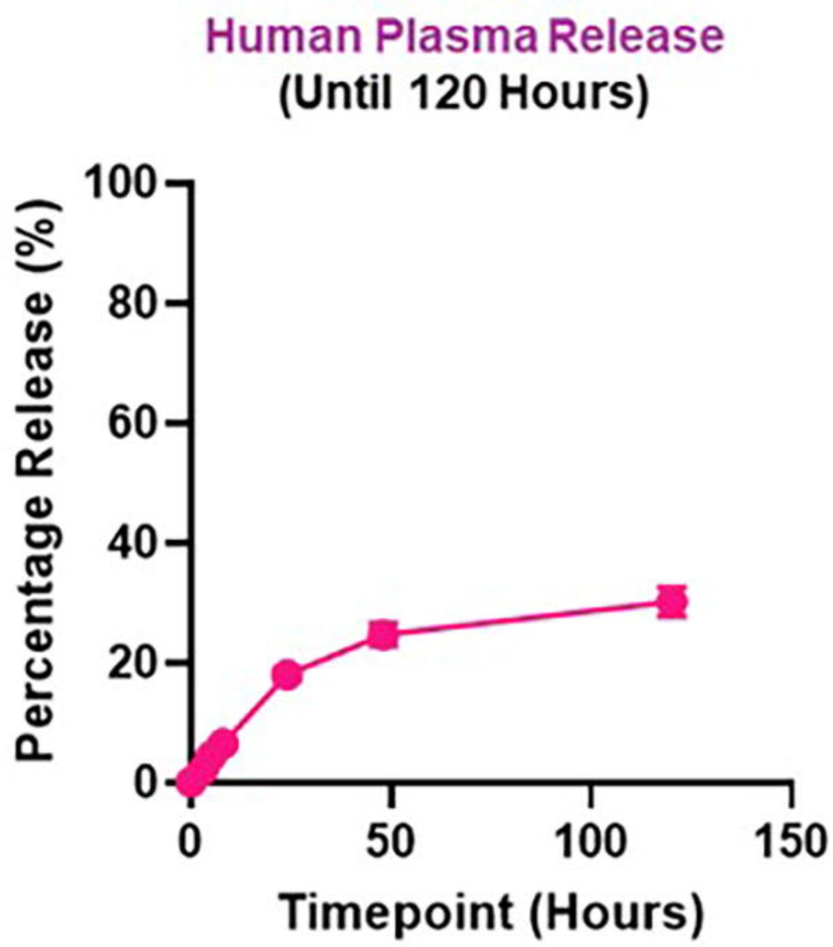

A

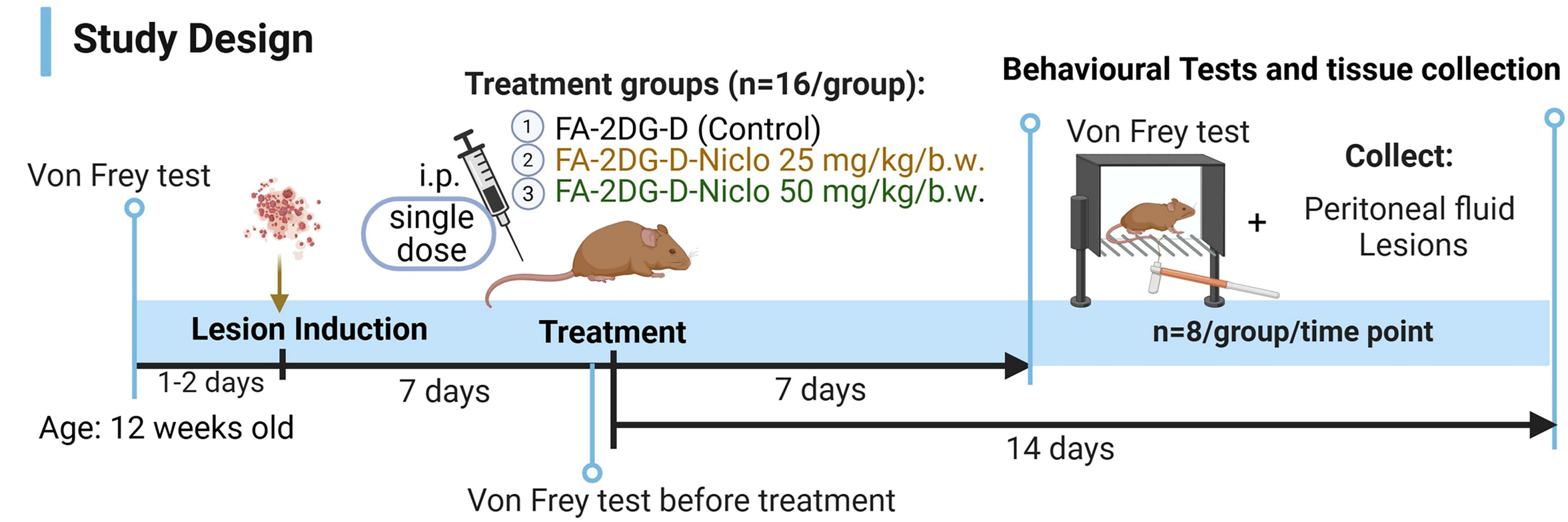
Study Design
Treatment groups (n=16/group):
1 FA-2DG-D (Control)
2 FA-2DG-D-Niclo 25 mg/kg/b.w.
3 FA-2DG-D-Niclo 50 mg/kg/b.w.
Behavioural Tests and tissue collection
Von Frey test
i.p.
single dose
Von Frey test
Collect:
Peritoneal fluid
Lesions
+
Lesion Induction
Treatment
n=8/group/time point
1-2 days
7 days
7 days
Age: 12 weeks old
14 days
Von Frey test before treatment

B

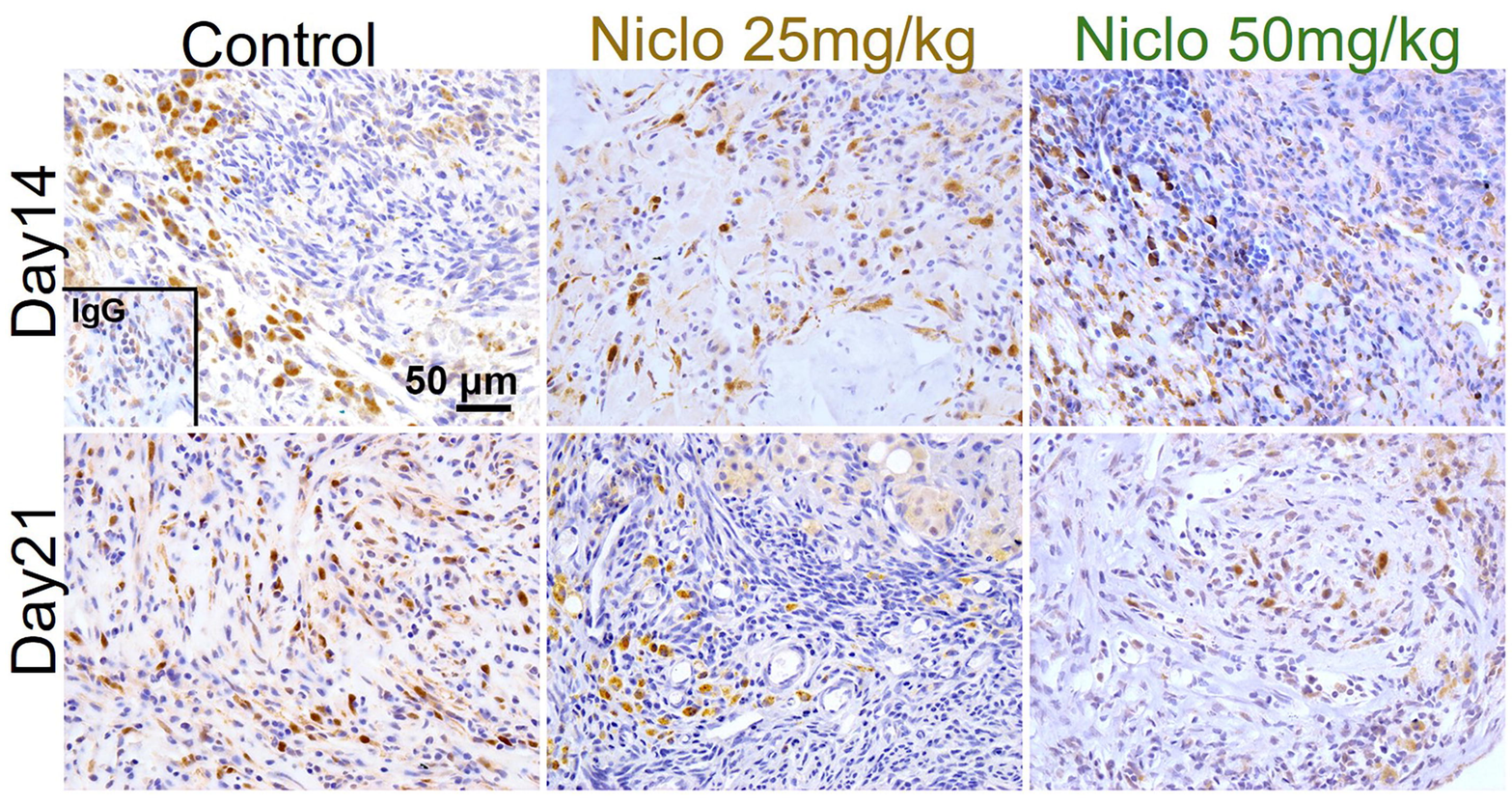
Control
Niclo 25mg/kg
Niclo 50mg/kg
Day14
Day21
IgG
50 µm

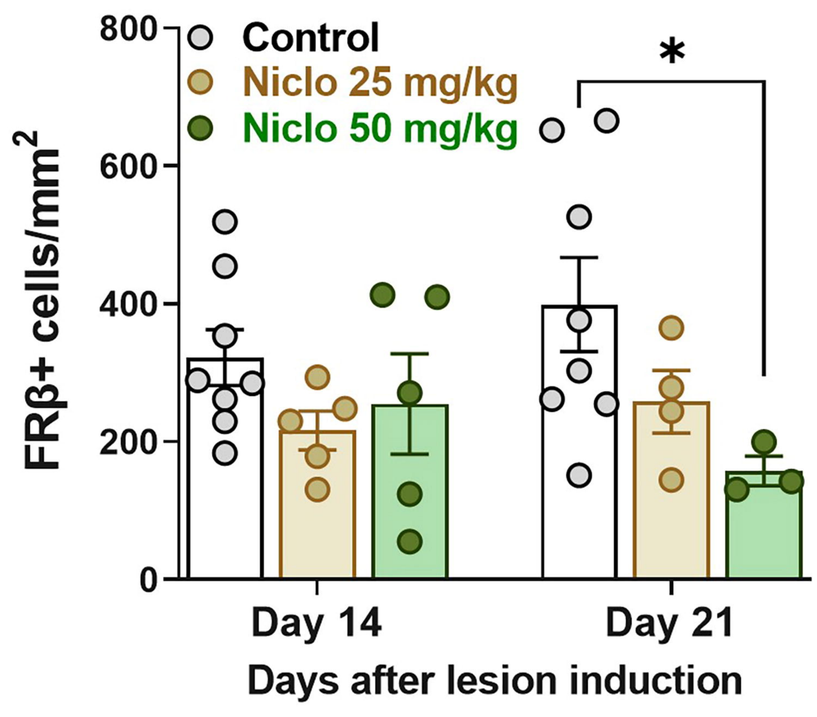
Control
Niclo 25 mg/kg
Niclo 50 mg/kg
FRβ+ cells/mm2
800
600
400
200
0
*
Day 14
Day 21
Days after lesion induction

C

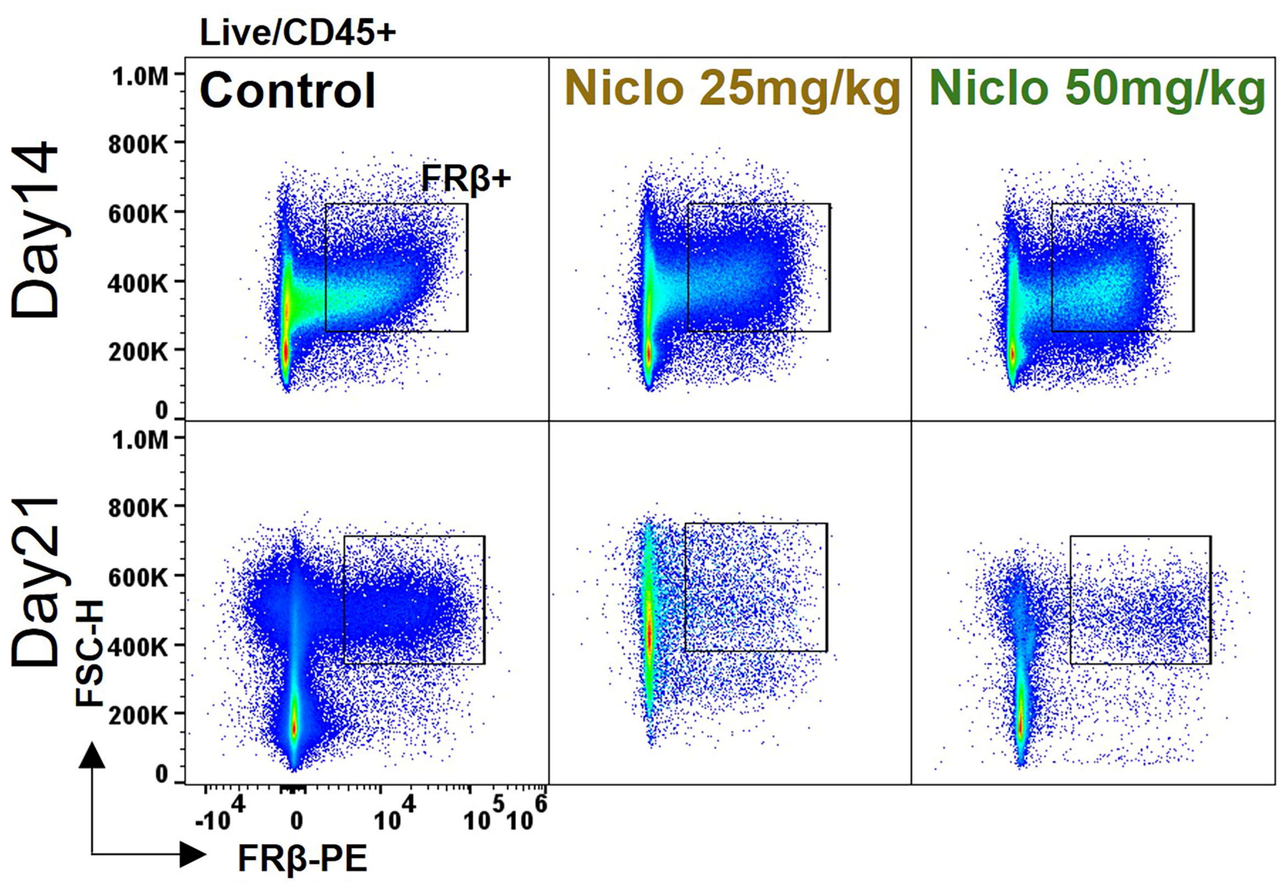
Live/CD45+
Control
Niclo 25mg/kg
Niclo 50mg/kg
Day14
Day21
FRβ+
1.0M
800K
600K
400K
200K
0
FSC-H
FRβ-PE

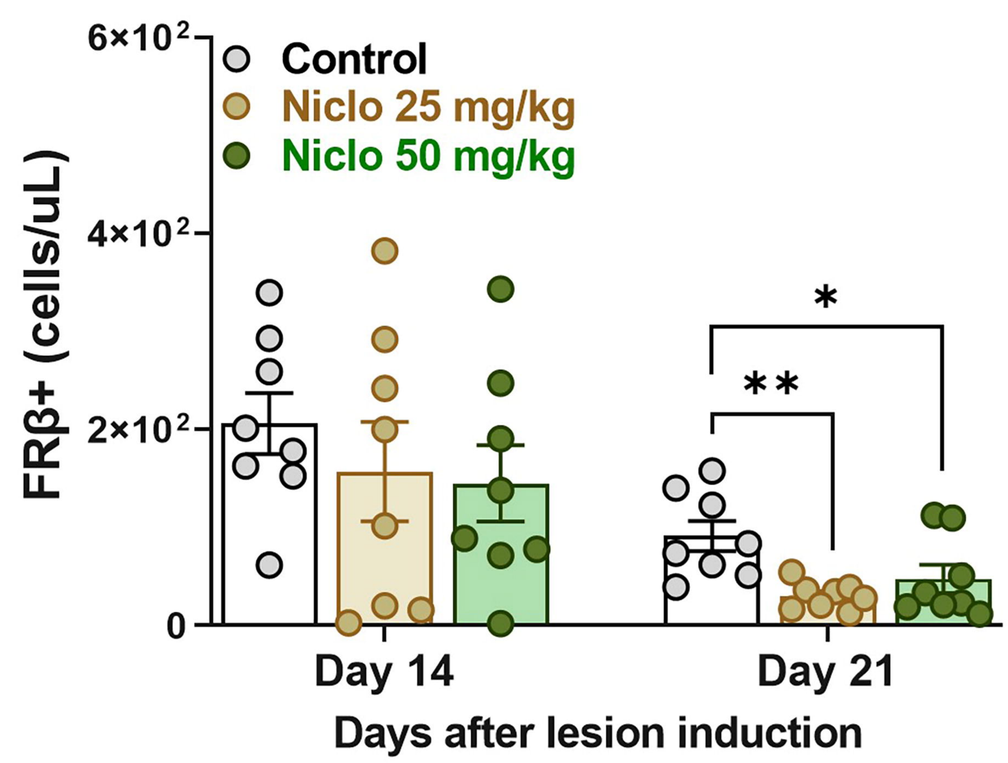
Control
Niclo 25 mg/kg
Niclo 50 mg/kg
FRβ+ (cells/uL)
6×10²
4×10²
2×10²
0
*
**
Day 14
Day 21
Days after lesion induction

A

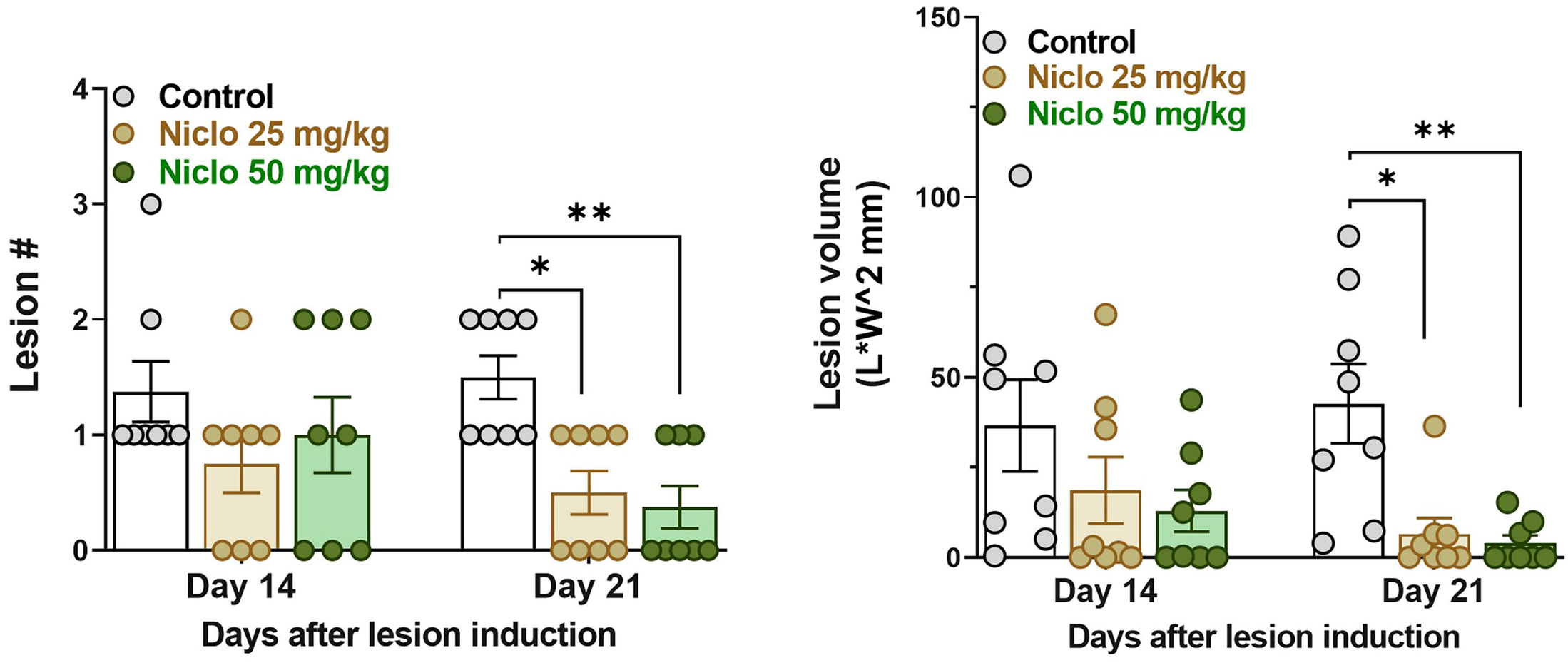
Control
Niclo 25 mg/kg
Niclo 50 mg/kg
Lesion #
Day 14
Day 21
Days after lesion induction
Lesion volume (L*W^2 mm)

B

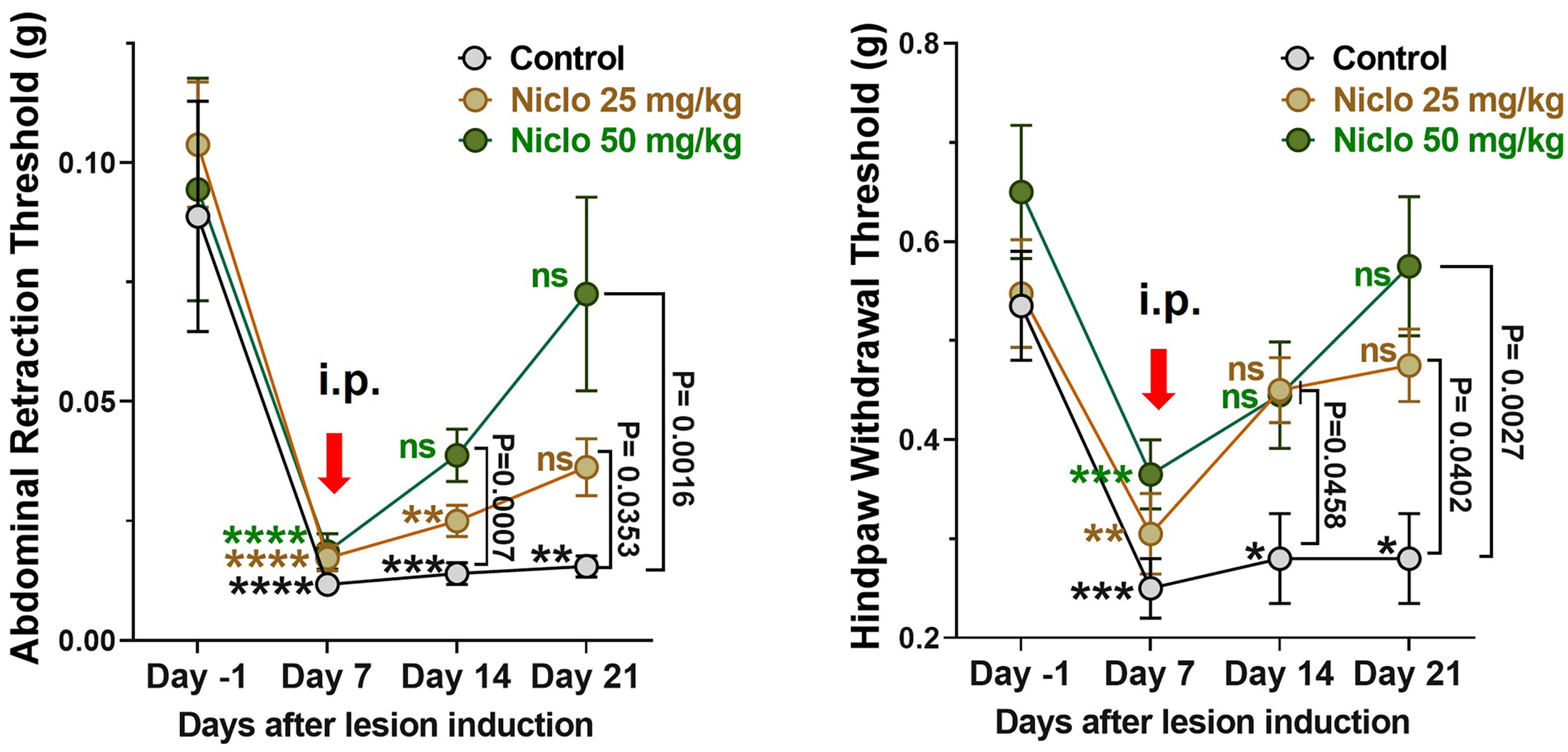
Control
Niclo 25 mg/kg
Niclo 50 mg/kg
Abdominal Retraction Threshold (g)
Hindpaw Withdrawal Threshold (g)
i.p.
ns
P= 0.0016
P= 0.0353
P=0.0007
P= 0.0027
P= 0.0402
P=0.0458
Day -1
Day 7
Day 14
Day 21
Days after lesion induction